# Final Report for Summer Internship 2020
# Part I: Theory and Experiments with HouckLab

Harshvardhan K. Babla
*Advised By*: Tudor-Alexandru Petrescu, Alexandre Blais

September 9, 2020

## Contents

**Acknowledgements**

I'd like to thank Prof. Blais and Alex for their continuous support and advice through the summer. Even though I wasn't able to be in Sherbrooke in person, they truly made sure that I had an incredibly fulfilling experience remotely.

Prof. Blais, I've learnt so much from the way you think about and effortlessly explain scientific concepts. Even though its only been a few months, but you've greatly shaped the way I will approach research going forward. Thank you for also making sure I felt part of the group even though I was miles away.

There were many times when I was stuck on a problem or completely confused about how to proceed. I would never have gotten through those times without Alex's support, advice, and theoretical acumen. Answering my questions and helping me debug code last into the evening, Alex has been one of the most dedicated advisors I've ever had.

I'd like to thank Maxime Dion at the IBM Q Hub in Sherbrooke for several insightful discussions with understanding experimental data, as well as navigating through the IBM Quantum Experience. Thanks to Alex Place and Pranav Mundada, in the HouckLab at Princeton, for fabricating and measuring a device for this experiment. This project would not have been possible without perspicacious conversations with Andrei Vrajitoarea (Princeton), Shantanu Mundhada (Yale), Abraham Asfaw (IBM), and Thomas Alexander (IBM).

Last but certainly not least, thank you to all the other members of the TheSQuaD group - Agustin di Paolo, Alexandre Choquette, Camille Le Calonnec, Catherine Leroux, Elie Genois, Joachim C., Jonathan Gross, and Ross Shillito - for making me feel very welcome within the group even though I couldn't be there in person.

# 1 Introduction

The goal of this project was to characterize the trend between the qubit's $T_1$ and the cavity population, $\bar{n}$. These are my notes the papers I read and the concepts I learnt over the summer. Starting from diagonalization of the Jaynes-Cummings Hamiltonian in the dispersive regime up to calibrating $\bar{n}$ from the qubit-spectrum.

The last chapter contains the crux of the experimental analysis for calibrating $\bar{n}$. Please refer to the attached Mathematica and Jupyter Notebooks for the code corresponding to this analysis.

The appendices contain some key derivations I worked through this summer, while reading seminal papers on Circuit QED.

Please refer to Part II, which is a description of my results from my Qiskit Open-Pulse.

# 2 Circuit Quantum Electrodynamics (Circuit QED)

## 2.1 The Jaynes-Cummings Hamiltonian

$$\boxed{\hat{H}_{JC} = \frac{1}{2}\hbar\omega_q\hat{\sigma}_z + \hbar\omega_c\left(\hat{a}^\dagger\hat{a} + \frac{1}{2}\right) + \hbar g\left(\hat{\sigma}_+\hat{a} + \hat{\sigma}_-\hat{a}^\dagger\right)} \tag{1}$$

$$\text{where} \qquad g = -\frac{1}{2}\Omega_0 = \frac{-\mathcal{P}_{ge}}{\hbar}\sqrt{\frac{\hbar\omega_c}{\epsilon_0 V}}\sin\left(\frac{\omega_c x_0}{c}\right) \tag{2}$$

## 2.2 Uncoupled Eigenstates

If we ignore the interaction term, $\hbar g V_+ = \hbar g\left(\hat{a}^\dagger\hat{a} + \frac{1}{2} + \hbar g\left(\hat{\sigma}_+\hat{a} + \hat{\sigma}_-\hat{a}^\dagger\right)\right)$, then the qubit and cavity essentially exist in seperate Hilbert spaces. As such, the eigenstates are simply the tensor product states between the cavity's Fock basis, $\{|n\rangle \mid \forall n \in \mathbb{Z}, n \geq 0\}$ and the TLS eigenstates $\{|g\rangle, |e\rangle\}$, with eigenenergies $E_{g/e,n}$ [1].

$$|n,g\rangle = |n\rangle \otimes |g\rangle \qquad\qquad |n,e\rangle = |n\rangle \otimes |e\rangle \tag{3a}$$

$$E_{g,n} = -\frac{1}{2}\hbar\omega_q + \hbar\omega_c\left(n + \frac{1}{2}\right) \qquad\qquad E_{e,n} = +\frac{1}{2}\hbar\omega_q + \hbar\omega_c\left(n + \frac{1}{2}\right) \tag{3b}$$

When the system is nearly resonant, i.e. $|\Delta| = |\omega_q - \omega_c| \ll \omega_c$, then the uncoupled eigenstates $|n,g\rangle$ and $|n-1,e\rangle$ are nearly degenerate. In other words, an excitation stored in the cavity is nearly equivalent to one stored in the qubit. The state corresponding to the qubit in the ground state and the cavity in vacuum, $|0,g\rangle$, is the only unpaired state [1].

These states can be organized into a ladder of doublets, as shown in Figure 2.2, where the $n^{th}$ doublet store $n$ elementary excitations either as $n$ field quanta or $n-1$ field quanta and one qubit (or atomic) quantum. The operator $\hat{N} = \hat{a}^\dagger\hat{a} + \hat{\sigma}_+\hat{\sigma}_-$ represents the total number of elementary excitations [1].

## 2.3 Dressed States

Now we can consider the full Jaynes-Cummings Hamiltonian given by Equation 2. Observe that $\hat{H}_{JC}$ commutes with the excitation number operator $\hat{N}$. This implies that the total number of

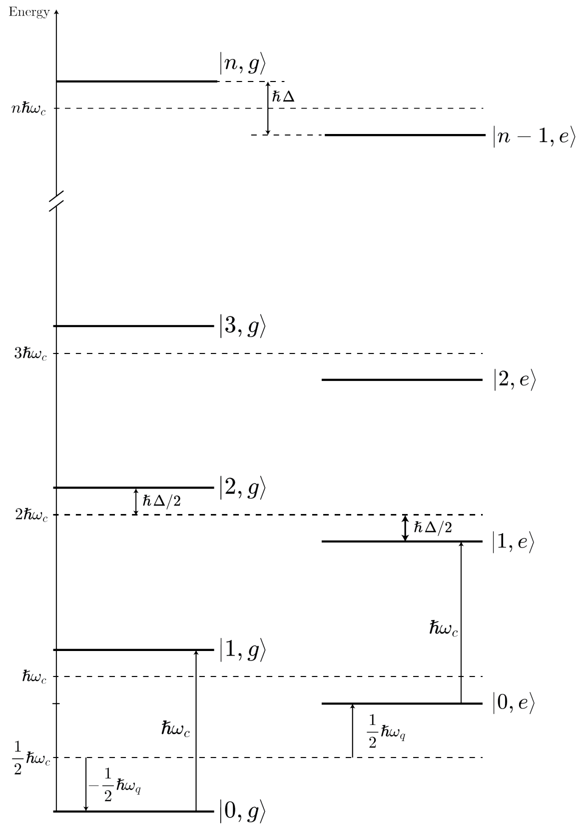


Figure 1: Uncoupled qubit-cavity eigenenergies, for $\Delta < 0$, organized as a ladder. Apart from the ground state $|0, g\rangle$, the eigenenergies pair into doublets where the total excitation number is conserved. In each doublet, the states $|n-1, g\rangle$ and $|n, e\rangle$ are seperated by $\hbar\Delta$. The doublets are seperated from each other by $\hbar\Delta$

excitations is conserved, and the coupling term $\hat{V_+}$ only causes an interaction within each doublet. This corresponds to our physical intuition that the excitation number is conserved when the cavity and qubit exchange a photon.

This allows us to restrict ourselves to the $n^{th}$ doublet only. The Hamiltonian restricted to the basis $\{|n, g\rangle, |n-1, e\rangle\}$ is:

$$\hat{H}_n = \hbar n\omega_c \hat{\mathbb{1}} - \frac{1}{2}\hbar \begin{bmatrix} \Delta & 2g\sqrt{n} \\ 2g\sqrt{n} & -\Delta \end{bmatrix}$$

This $2 \times 2$ matrix is simply diagonalized, to get the exact eigenvalues (given by Equation 4) and eigenstates (given by Equation 5). Figure 2.3 shows the eigenenergies as a function of the qubit-cavity detuning. Observe that as $\Delta/g \to \infty$, the states dressed states tend towards the uncoupled states. This can be understood as the qubit and cavity becoming so far detuned that any interaction between them is supressed [1, 2].

$$\boxed{E_{\pm,n} = \hbar n\omega_c \pm \hbar\frac{\Delta}{2}\sqrt{1 + 4n\left(\frac{g}{\Delta}\right)^2}} \tag{4}$$

$$|n_+\rangle = \sin\theta_n |n, g\rangle + \cos\theta_n |n-1, e\rangle \tag{5a}$$
$$|n_-\rangle = \cos\theta_n |n, g\rangle - \sin\theta_n |n-1, e\rangle \tag{5b}$$

where

$$\tan(2\theta_n) = \frac{2g\sqrt{n}}{\Delta} \tag{6}$$

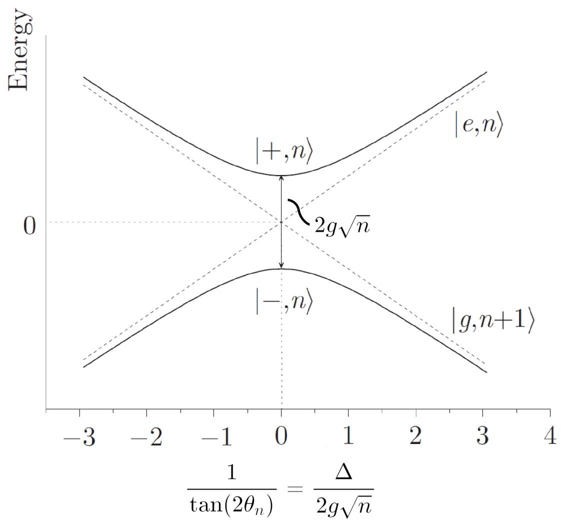


Figure 2: The Dressed State energies as a function of the relative detuning $\frac{\Delta}{2g\sqrt{n}}$. The uncoupled energies are represented as dotted lines. Sourced from [1].

# 3 Strong Dispersive Regime

It is most common to work in the dispersive regime of Circuit QED, where $|\Delta| \gg g$. Here the dressed states are only weakly entangled between the qubit and cavity, thus retaining much of their individual characters [2]. As will be shown in Equations 9 and 10, the interaction term in the dispersive regime can be expressed as a cavity-dependant shift on the qubit frequency or a qubit-dependant shift on the cavity frequency. This allows us to measure the qubit with minimal backaction (a Quantum Non-Demolition Measurement) by probing the cavity response.

In the strong dispersive regime, $\frac{g}{|\Delta|} \ll 1$, thus we can obtain the approximate solutions for the eigenenergies by Taylor expanding Equation 4, to second order in $\frac{g}{\Delta}$.

$$\begin{aligned} E_{\pm,n} &= \hbar n\omega_c \pm \hbar\frac{\Delta}{2}\sqrt{1+4n\left(\frac{g}{\Delta}\right)^2} \\ &= \hbar n\omega_c \pm \hbar\frac{\Delta}{2}\left[1+\frac{2ng^2}{\Delta^2}+\mathcal{O}\left(\frac{g^4}{\Delta^4}\right)\right] \\ &\approx \hbar n(\omega_c \pm \chi) \pm \frac{\hbar}{2}\Delta \end{aligned} \tag{7}$$

where we've defined $\chi = \frac{g^2}{\Delta}$. However, this approximation only holds if $4n\left(\frac{g}{\Delta}\right)^2$ isn't of order one. In other words, the approximation is valid for excitation numbers $n \ll n_{crit} = \frac{\Delta^2}{4g^2}$ [2, 3, 4].

Similarly, we can find the eigenstates of in the dispersive regime, by Taylor expanding Equation 5 to second order in $\frac{g}{\Delta}$ (using Wolfram Alpha).

$$\cos\left(\frac{1}{2}\arctan\left(\frac{2g\sqrt{n}}{\Delta}\right)\right) = 1-\frac{n}{2}\left(\frac{g}{\Delta}\right)^2+\mathcal{O}\left(\frac{g^4}{\Delta^4}\right)$$
$$\sin\left(\frac{1}{2}\arctan\left(\frac{2g\sqrt{n}}{\Delta}\right)\right) = \sqrt{n}\left(\frac{g}{\Delta}\right)+\mathcal{O}\left(\frac{g^3}{\Delta^3}\right)$$

$$|n_+\rangle \approx \frac{g\sqrt{n}}{\Delta}|n,g\rangle + \left(1-\frac{ng^2}{2\Delta^2}\right)|n-1,e\rangle \tag{8a}$$

$$|n_-\rangle \approx \left(1-\frac{ng^2}{2\Delta^2}\right)|n,g\rangle - \frac{g\sqrt{n}}{\Delta}|n-1,e\rangle \tag{8b}$$

This shows that the dressed states are weakly entangled qubit-cavity states, with a high probability of the wavefunction lying in the same place as the qubit-cavity excitation. Particularly, $|n_+\rangle$ represents a high probability of finding the excitation in the cavity and $|n_-\rangle$ represents a high probability of finding an exited qubit.

Alternatively, we can diagonalize the Hamiltonian using a unitary transformation [3] using the Schrieffer-Wolff Transformation, hoping to understand the physics of the system better.

## 3.1 Schrieffer-Wolff Transformation (Linear Regime)

We can write the JC Hamiltonian as $\hat{H} = \hat{H}_0 + \hbar g \hat{V}_+$, where $\hat{H}_0$ is the uncoupled Hamiltonian and $V_+ = \hat{\sigma}_+ \hat{a} + \hat{\sigma}_- \hat{a}^\dagger$ is the interaction term. The uncoupled eigenstates found in section 2.2, exactly diagonalize $H_0$ (i.e. $\langle n, z_1 | H_0 | m, z_2 \rangle = E_{n,z} \delta_{nm} \delta_{z_1 z_2}$, for $z_1, z_2 \in \{g, e\}$). However, the interaction is purely off-diagonal $\langle n, z | V_+ | n, z \rangle = 0 \quad \forall\, n \in \mathbb{Z}_+, z \in \{g, e\}$.

The Schrieffer-Wolff Transformation is a unitary transformation which diagonalizes $\hat{H}_{JC}$. This transformation is written as $\hat{H}' = \hat{U}^\dagger_{SW} \hat{H} \hat{U}_{SW} = e^{\hat{S}} \hat{H} e^{-\hat{S}}$, where $\hat{S}$ is an arbitrary time-independent operator.

$\hat{H}'$ can be expanded using the Baker-Campbell-Haussdorf formula:

$$\hat{H}' = e^{\hat{S}} \hat{H} e^{-\hat{S}} = \hat{H} + [\hat{S}, \hat{H}] + \frac{1}{2!}[\hat{S}, [\hat{S}, \hat{H}]] + \frac{1}{3!}[\hat{S}, [\hat{S}, [\hat{S}, \hat{H}]]] + \dots$$

To approximately diagonalize the Hamiltonian to second order in the small parameter $\frac{g}{\Delta}$, we can choose $\hat{S} = \frac{g}{\Delta} \hat{V}_- = \frac{g}{\Delta} \left( \hat{\sigma}_+ \hat{a} - \hat{\sigma}_- \hat{a}^\dagger \right)$, such that $[\hat{H}_0, \hat{S}] = \hbar g \hat{V}_+$. This way, we're able to write down the effective Hamiltonian in the dispersive regime, to first order in $\chi = \frac{g^2}{\Delta}$, as in Equation 9. The complete derivation is described in Appendix B.

$$\boxed{\hat{H}_{disp} = \frac{1}{2} \hbar \omega_q \hat{\sigma}_z - \hbar \left( \omega_c + \chi \hat{\sigma}_z \right) \left( \hat{a}^\dagger \hat{a} + \frac{1}{2} \right) - \frac{1}{2} \hbar \chi} \tag{9}$$

This Hamiltonian can be given complementary physical implementations, depending on which interacting subsystems we're observing [2, 1].

The Hamiltonian as arranged above can be interpreted as a pull on the cavity frequency dependant the qubit state. With the qubit in the $|g\rangle$ state, the cavity frequency is pulled to $\omega_c - \chi$. On the other hand, for a qubit in the $|e\rangle$ state the cavity is pulled to $\omega_c + \chi$. This effect can be interpreted as dielectric inside the cavity. The state of the qubit can be related to the refractive index of the dielectric. Changing the state of the qubit changes the effective cavity length and hence the mode frequency [2, 1].

Alternatively, we can rearrange the Hamiltonian, as below, to observe a light-shift on the qubit frequency.

$$\boxed{\hat{H}_{disp} = \frac{1}{2} \hbar \left[ \omega_q - 2\chi \left( \hat{a}^\dagger \hat{a} + \frac{1}{2} \right) \right] \hat{\sigma}_z + \hbar \omega_c \left( \hat{a}^\dagger \hat{a} + \frac{1}{2} \right) - \frac{1}{2} \hbar \chi} \tag{10}$$

The shift on the qubit transition frequency can be interpreted as having two contributions. The first contribution, $-2\chi \hat{a}^\dagger \hat{a}$ is a photon-number dependant Stark shift. The second $+\chi$ is a Lamb-shift, induced by the $\frac{1}{2}$ photon observed in the cavity vacuum [1].

## 3.2 Exact Diagonalization

Ref. [3] observes that even for a small number of photons $\overline{n} \approx 0.08 n_{crit}$ in the resonator, visible differences can be seen in the simulations of the effective dispersive Hamiltonian and the true Hamiltonian. This motivates them to exactly diagonalize the dispersive Hamiltonian. The following derivation, fully detailed in Appendix C, is inspired by [3].

Just as in the linear regime, we transform the Hamiltonian using the unitary $e^{\hat{S}}$ and expand it using the BCH formula. However, for a complete diagonalization we set $\hat{S} = f(\hat{N})\hat{V}_-$, where $\hat{N} = \hat{a}^\dagger\hat{a} + \hat{\sigma}_+\hat{\sigma}_-$ is the total excitation number operator and

$$f(\hat{N}) = \frac{-\arctan(2\frac{g}{\Delta}\sqrt{\hat{N}})}{2\sqrt{\hat{N}}}$$

This ensures that off-diagonal interaction term proportional to $\hat{V}_+$ is eliminated. With this, we can write the exact diagonal form of the dispersive Hamiltonian as:

$$\boxed{\hat{H}' = \hat{H}_0 - \frac{1}{2}\hbar\Delta\left(1 - \sqrt{1 + 4\hat{N}\left(\frac{g}{\Delta}\right)^2}\right)\hat{\sigma}_z} \tag{11}$$

Observe that this solution identically corresponds to the exact eigenenergies found in Equation 4. Using this result, we can define the Lamb and AC-Stark shifts as

$$\delta_L \equiv \langle 0,e|\hat{H}'|0,e\rangle - \langle 0,g|\hat{H}'|0,g\rangle - \hbar\omega_q$$

$$= -\frac{1}{2}\hbar\Delta\left(1 - \sqrt{1+4\left(\frac{g}{\Delta}\right)^2}\right) \tag{12}$$

$$\approx \hbar\left[\frac{g^2}{\Delta}\left(1 - \frac{g^2}{\Delta^2}\right)\right] + \mathcal{O}\left(\left(\frac{g}{\Delta}\right)^5\right) \tag{13}$$

$$\delta_S(n) \equiv \langle n,e|\hat{H}'|n,e\rangle - \langle n,g|\hat{H}'|n,g\rangle - \delta_L - \hbar\omega_q$$

$$= \frac{1}{2}\hbar\Delta\left(\sqrt{1+4(n+1)\left(\frac{g}{\Delta}\right)^2} + \sqrt{1+4n\left(\frac{g}{\Delta}\right)^2} - 1 - \sqrt{1+4\left(\frac{g}{\Delta}\right)^2}\right) \tag{14}$$

$$\approx \hbar n\left[\frac{g^2}{\Delta}\left(1 - \frac{g^2}{\Delta^2}\right)\right] + \hbar n^2\left(-\frac{g^4}{\Delta^3}\right) + \mathcal{O}\left(\left(\frac{g}{\Delta}\right)^5\right) \tag{15}$$

We can define the modified value of Lamb and Stark shift per photon as

$$\chi \equiv \frac{g^2}{\Delta}\left(1 - \frac{g^2}{\Delta^2}\right) \tag{16}$$

and the third-order squeezing term ($\sim n^2$) amplitude as

$$\zeta \equiv -\frac{g^4}{\Delta^3} \tag{17}$$

Then, to third order in $\frac{g}{\Delta}$, the dispersive Hamiltonian can be written as

$$\boxed{\hat{H}' \approx \frac{1}{2}\hbar\left[\omega_q - 2\chi\left(\hat{a}^\dagger\hat{a} + \frac{1}{2}\right)\right]\hat{\sigma}_z + \hbar(\omega_c + \zeta)\left(\hat{a}^\dagger\hat{a} + \frac{1}{2}\right) + \hbar\zeta\left(\hat{a}^\dagger\hat{a}\right)^2\hat{\sigma}_z} \tag{18}$$

### 3.3 Cavity Pull as a Function of the Cavity Population

Just as before, we can rearrange the Hamiltonian above to show a shift in the cavity frequency.

$$\boxed{\hat{H}' \approx \frac{1}{2}\hbar\left(\omega_q - \chi\right)\hat{\sigma}_z + \hbar\left[\omega_c + \zeta - \left(\chi + \zeta\hat{a}^\dagger\hat{a}\right)\hat{\sigma}_z\right]\hat{a}^\dagger\hat{a} + \frac{1}{2}\hbar(\omega_c + \zeta)} \tag{19}$$

Observe that the pull on the cavity frequency is not only dependant on the state of the qubit, but also on the number of photons present in the cavity.

The linear dependance of the cavity-pull on the photon-number is only valid up to third order in $\frac{g}{\Delta}$. In other words, for $\bar{n} \ll n_{crit}$. The exact shift in the cavity frequency is given by

$$\begin{aligned}\delta_C(n, |g\rangle) &\equiv \langle n+1, g|\hat{H}'|n+1, g\rangle - \langle n, g|\hat{H}'|n, g\rangle - \hbar\omega_c \\ &= \frac{1}{2}\hbar\Delta\left(\sqrt{1+4(n+1)\left(\frac{g}{\Delta}\right)^2} - \sqrt{1+4n\left(\frac{g}{\Delta}\right)^2}\right)\end{aligned} \tag{20}$$

$$\begin{aligned}\delta_C(n, |e\rangle) &\equiv \langle n, e|\hat{H}'|n, e\rangle - \langle n-1, e|\hat{H}'|n-1, e\rangle - \hbar\omega_c \\ &= -\frac{1}{2}\hbar\Delta\left(\sqrt{1+4(n+1)\left(\frac{g}{\Delta}\right)^2} - \sqrt{1+4n\left(\frac{g}{\Delta}\right)^2}\right)\end{aligned} \tag{21}$$

Figure 3.3 shows the cavity pull as a function of the mean number of photons in the cavity, $\bar{n}$ for the qubit in the ground (blue) and excited (red) states. The figure compares the cavity pull from the exact diagonalization (solid line), given by Equations 20 and 21, to the ones from the first-order (dashed line) and third-order (dotted line) approximations of the dispersive Hamiltonian (dashed line), given by Equations 9 and 19 respectively. This result qualitatively matches the results from Ref. [5]. [1]

The first-order approximation of the dispersive Hamiltonian predicts a constant cavity pull, as such significantly differs from the true value well before $n_{crit}$. On the other hand, the third-order approximation predicts a linear relationship between the cavity pull and $\bar{n}$, closely approximating the true trend.

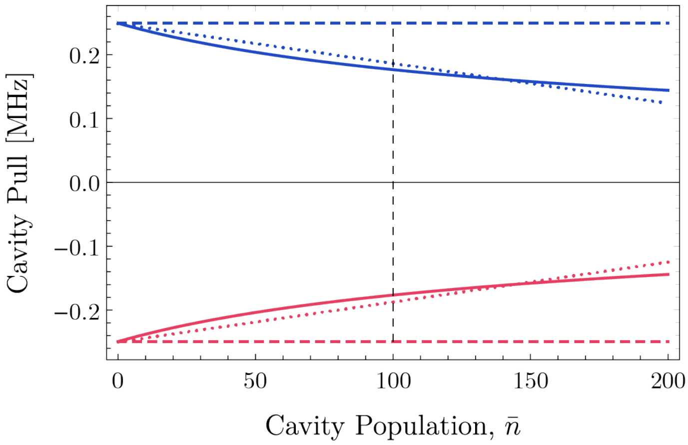


Figure 3: The shift on the cavity frequency (Cavity Pull) as a function of the mean photon number in the cavity (Cavity Population), for a system with $\Delta/2\pi = 100$ MHz and $g/2\pi = 5$ MHz. The relationship shown depends on whether the qubit is in the ground (blue) or excited state (red). The solid, dashed, and dotted lines give this relationship for the exact diagonalization, first-order approximation, and third-order approximation respectively. The vertical line indicates $n_{crit} \equiv \frac{\Delta^2}{4g^2} = 100$ photons.

## 4 Drive Terms on the Hamiltonian

We can control and readout the qubit by applying coherent microwave tones on the system. These are represented in the drive Hamiltonian, $\hat{H}_d$, as superposition of a measurement tone on

[1] Refer to the attached Mathematica `notebook cavity_pull_vs_nbar.nb` for the code to generate Figure 3.3.

the and a drive tone.

$$\hat{H}_d = \epsilon_m(t)\left(\hat{a}e^{i\omega_m t} + \hat{a}^\dagger e^{-i\omega_m t}\right) + \epsilon_d(t)\left(\hat{a}e^{i\omega_d t} + \hat{a}^\dagger e^{-i\omega_d t}\right) \tag{22}$$

where $\epsilon_m(t)$ and $\epsilon_d(t)$ are the measurement and qubit-drive pulse envelopes respectively. $\omega_m$ and $\omega_d$ are the corresponding frequencies of the applied pulses. Usually we measure at the cavity frequency ($\Delta_{cm} \equiv \omega_c - \omega_m \approx 0$) and drive at the qubit frequency ($\Delta_{qd} \equiv \omega_q - \omega_d \approx 0$).

We can use the Schrieffer-Wolff transformation to express $\hat{H}_{drive}$ in first order in $\frac{g}{\Delta}$.

$$\begin{aligned}\hat{H}'_{drive} \equiv& \,\hat{\mathcal{U}}^\dagger_{SW}\hat{H}_d\hat{\mathcal{U}}_{SW}\\ =& \,\epsilon_m(t)\left(\hat{a}e^{i\omega_m t} + \hat{a}^\dagger e^{-i\omega_m t}\right) - \frac{g}{\Delta}\epsilon_m(t)\left(\hat{\sigma}_- e^{i\omega_m t} + \hat{\sigma}_+ e^{-i\omega_m t}\right)\\ &+ \epsilon_d(t)\left(\hat{a}e^{i\omega_d t} + \hat{a}^\dagger e^{-i\omega_d t}\right) - \frac{g}{\Delta}\epsilon_d(t)\left(\hat{\sigma}_- e^{i\omega_d t} + \hat{\sigma}_+ e^{-i\omega_d t}\right)\end{aligned} \tag{23}$$

To eliminate the rotating terms, we can transform into the Interaction picture given by the unitary operator

$$\hat{\mathcal{U}}(t) = \exp\left\{-i\left[\omega_m\left(\hat{a}^\dagger\hat{a} + \frac{1}{2}\right) + \frac{1}{2}\omega_d\hat{\sigma}_z\right]t\right\}$$

This transformation ensures that

$$\hat{a} \longrightarrow \hat{\mathcal{U}}^\dagger(t)\,\hat{a}\,\hat{\mathcal{U}}(t) = \hat{a}e^{-i\omega_m t} \qquad\qquad \hat{\sigma}_- \longrightarrow \hat{\mathcal{U}}^\dagger(t)\,\hat{\sigma}_-\,\hat{\mathcal{U}}(t) = \hat{\sigma}_- e^{-i\omega_d t}$$

Thus, in the interaction picture the drive Hamiltonian becomes

$$\begin{aligned}\hat{H}'_{d,int} \equiv& \,\hat{\mathcal{U}}^\dagger\hat{H}'_d\hat{\mathcal{U}}\\ =& \,\epsilon_m(t)\left(\hat{a} + \hat{a}^\dagger\right) - \frac{g}{\Delta}\epsilon_m(t)\left(\hat{\sigma}_- e^{i(\omega_m-\omega_d)t} + \hat{\sigma}_+ e^{-i(\omega_m-\omega_d)t}\right)\\ &+ \epsilon_d(t)\left(\hat{a}e^{-i(\omega_m-\omega_d)t} + \hat{a}^\dagger e^{i(\omega_m-\omega_d)t}\right) - \frac{g}{\Delta}\epsilon_d(t)\hat{\sigma}_x\end{aligned} \tag{24}$$

Where we've used the identity $\hat{\sigma}_- + \hat{\sigma}_+ = \hat{\sigma}_x$. Consider the term $\omega_m - \omega_d = (\omega_c - \Delta_{cm}) - (\omega_q - \Delta_{qd}) = \Delta - \Delta_{cm} - \Delta_{qd} \approx \Delta$. Thus, the corresponding terms are rotating very fast, which we may ignore with the rotating wave approximation.

Finally, to write the complete Hamiltonian, we must express the undriven Hamiltonian in this interaction picture. $\hat{H}'$ from Equation 9 commutes with $\hat{\mathcal{U}}(t)$, however to satisfy the Schrodinger Equation in the Interaction picture we must consider the time-derivative of $\hat{\mathcal{U}}(t)$.

$$\begin{aligned}\hat{H}'_{int} =& \,\hat{\mathcal{U}}^\dagger\left(\hat{H}' + \hat{H}'_d\right)\hat{\mathcal{U}} - i\hbar\,\hat{\mathcal{U}}\,\frac{\mathrm{d}\hat{\mathcal{U}}^\dagger}{\mathrm{d}t}\\ =& \,\hat{H}' + \hat{H}'_{d,int} - \hbar\left[\omega_m\left(\hat{a}^\dagger\hat{a} + \frac{1}{2}\right) + \frac{1}{2}\omega_d\hat{\sigma}_z\right]\end{aligned}$$

Therefore, in the interaction picture, the complete driven dispersive Hamiltonian (to first order in $\frac{g}{\Delta}$) is given by

$$\boxed{\frac{\hat{H}'_{int}}{\hbar} = \frac{\Delta_{qd}}{2}\hat{\sigma}_z + (\Delta_{cm} - \chi\hat{\sigma}_z)\left(\hat{a}^\dagger\hat{a} + \frac{1}{2}\right) + \epsilon_m(t)(\hat{a} + \hat{a}^\dagger) + \Omega_d(t)\hat{\sigma}_x - \frac{1}{2}\chi} \tag{25}$$

where we've defined the effective drive on the qubit as $\Omega_d(t) = -\frac{g}{\Delta}\epsilon_d(t)$.

To perform a gate on the qubit, we can input a constant drive tone, $\Omega_d(t) = \frac{\theta}{2}$, such that the qubit evolves according to

$$\begin{aligned}\mathcal{U}_q(t) = e^{-i\hat{H}t/\hbar} &= e^{-i(\Delta_q\hat{\sigma}_z + \theta\hat{\sigma}_x)t/2}\\ &= \left[\cos(\Delta_q t)\hat{\mathbb{1}} + \sin(\Delta_q t)\hat{\sigma}_z\right]\left[\cos(\theta t)\hat{\mathbb{1}} + \sin(\theta t)\hat{\sigma}_x\right]\\ &= \cos(\Delta_q t)\cos(\theta t)\hat{\mathbb{1}} + \sin(\Delta_q t)\cos(\theta t)\hat{\sigma}_z\\ &\qquad + \cos(\Delta_q t)\sin(\theta t)\hat{\sigma}_x + i\sin(\Delta_q t)\sin(\theta t)\hat{\sigma}_y\end{aligned} \tag{26}$$

For example, to perform a bit-flip (X-gate), we can drive the qubit at $\Delta_{qd} = 0$, for a duration $\tau$ such that $\theta\tau = \frac{\pi}{2}$.

Similarly, the cavity can be populated using the coherent microwave tone $\epsilon(t)$. This is discussed in detail in Section 6.3.

# 5 Damping

## 5.1 The Lindblad Master Equation of the System

The density operator $\hat{\rho}$ fully describes any multi-particle system. The expectation value of any operator on this system is given by: $\langle\hat{B}\rangle = \text{trace}(\hat{\rho}\hat{B})$.

Any real physical system is never absolutely isolated, as the interactions of the system with the environment result in a dissipation of energy, causing non-unitary time-evolution such as decay and randomization of phase. The time-evolution of such a system (i.e. a microscopic quantum system coupled to a larger reservoir) is given by a Lindblad Master Equation. Each super-operator in the Lindblad Master Equation represents a non-unitary effect on the system, induced by the environment.

Equation 27 is a Linblad-type Master Equation to model a circuit QED system at zero temperature, that is coupled to its surroundings [6].

$$\boxed{\frac{\mathrm{d}}{\mathrm{d}t}\hat{\rho} = -\frac{i}{\hbar}[\hat{H},\hat{\rho}] + \kappa\mathcal{D}[\hat{a}]\hat{\rho} + \gamma_1\mathcal{D}[\hat{\sigma}_-]\hat{\rho} + \frac{\gamma_\phi}{2}\mathcal{D}[\hat{\sigma}_z]\hat{\rho}} \tag{27}$$

where the super-operator $\mathcal{D}[\hat{A}]$ acts on the density matrix $\hat{\rho}$ by

$$\mathcal{D}[\hat{A}]\hat{\rho} = \hat{A}\hat{\rho}\hat{A}^\dagger - \frac{1}{2}\hat{A}^\dagger\hat{A}\hat{\rho} - \frac{1}{2}\hat{\rho}\hat{A}^\dagger\hat{A}$$

Here $\hat{H}$ is the complete Hamiltonian given by Equation 25. The dissapators $\mathcal{D}[\hat{a}]$, $\mathcal{D}[\hat{\sigma}_-]$, and $\mathcal{D}[\hat{\sigma}_z]$ represent photon decay, qubit decay, and qubit decoherence respectively. The coefficients $\kappa$, $\gamma_1$, and $\gamma_\phi/2$ are the corresponding rates for these dissipation processes.

## 5.2 Cavity Bloch Equations

Ref [6] derive the 'Cavity-Bloch equations'(CBEs). These are a set of differential equations which approximately describe their system, without requiring that the Master equation be solved directly. They assume the dispersive Hamiltonian in the linear regime, given by Equation 9.

Equation 28 is the set of Cavity Bloch Equations corresponding to the Master Equation 27. Equations 28(c) and (d) are derived under the approximation $\langle\hat{a}^\dagger\hat{a}\hat{\sigma}_i\rangle \approx \langle\hat{a}^\dagger\hat{a}\rangle\langle\hat{\sigma}_i\rangle$, which should be valid for low photon numbers, where dephasing caused by photon shot noise is ignored. Similarly, Equations 28(e), (f) and (g) are true for the semi-classical approximation $\langle\hat{a}^\dagger\hat{a}\hat{a}\hat{\sigma}_i\rangle \approx \langle\hat{a}^\dagger\hat{a}\rangle\langle\hat{a}\hat{\sigma}_i\rangle$. The entire set of CBEs is derived in detailed in Appendix D.

$$\frac{\mathrm{d}}{\mathrm{d}t}\langle \hat{a} \rangle = -i\Delta_{cm}\langle \hat{a} \rangle - i\chi\langle \hat{a}\hat{\sigma}_z \rangle - i\epsilon_m + \frac{\kappa}{2}\langle \hat{a} \rangle \tag{28a}$$

$$\frac{\mathrm{d}}{\mathrm{d}t}\langle \hat{\sigma}_z \rangle = \Omega_d\langle \hat{\sigma}_y \rangle - \gamma_1(1 + \langle \hat{\sigma}_z \rangle) \tag{28b}$$

$$\frac{\mathrm{d}}{\mathrm{d}t}\langle \hat{\sigma}_x \rangle = -\left[\Delta_{qd} + 2\chi\left(\langle \hat{a}^\dagger \hat{a} \rangle + \frac{1}{2}\right)\right]\langle \hat{\sigma}_y \rangle - \gamma_2\langle \hat{\sigma}_x \rangle \tag{28c}$$

$$\frac{\mathrm{d}}{\mathrm{d}t}\langle \hat{\sigma}_y \rangle = \left[\Delta_{qd} + 2\chi\left(\langle \hat{a}^\dagger \hat{a} \rangle + \frac{1}{2}\right)\right]\langle \hat{\sigma}_x \rangle - \Omega_d\langle \hat{\sigma}_z \rangle - \gamma_2\langle \hat{\sigma}_y \rangle \tag{28d}$$

$$\frac{\mathrm{d}}{\mathrm{d}t}\langle \hat{a}\hat{\sigma}_z \rangle = -i\Delta_{cm}\langle \hat{a}\hat{\sigma}_z \rangle - i\chi\langle \hat{a} \rangle + \Omega_d\langle \hat{a}\hat{\sigma}_y \rangle - i\epsilon_m\langle \hat{\sigma}_z \rangle - \gamma_1\langle \hat{a} \rangle - \left(\gamma_1 + \frac{\kappa}{2}\right)\langle \hat{a}\hat{\sigma}_z \rangle \tag{28e}$$

$$\frac{\mathrm{d}}{\mathrm{d}t}\langle \hat{a}\hat{\sigma}_x \rangle = -i\Delta_{cm}\langle \hat{a}\hat{\sigma}_x \rangle - [\Delta_{as} + 2\chi(\langle \hat{a}^\dagger \hat{a} \rangle + 1)]\langle \hat{a}\hat{\sigma}_y \rangle - i\epsilon_m\langle \hat{\sigma}_x \rangle - \left(\gamma_2 + \frac{\kappa}{2}\right)\langle \hat{a}\hat{\sigma}_x \rangle \tag{28f}$$

$$\frac{\mathrm{d}}{\mathrm{d}t}\langle \hat{a}\hat{\sigma}_y \rangle = -i\Delta_{cm}\langle \hat{a}\hat{\sigma}_y \rangle - [\Delta_{as} + 2\chi(\langle \hat{a}^\dagger \hat{a} \rangle + 1)]\langle \hat{a}\hat{\sigma}_x \rangle - i\epsilon_m\langle \hat{\sigma}_y \rangle - \Omega_d\langle \hat{a}\hat{\sigma}_z \rangle - \left(\gamma_2 + \frac{\kappa}{2}\right)\langle \hat{a}\hat{\sigma}_y \rangle \tag{28g}$$

$$\frac{\mathrm{d}}{\mathrm{d}t}\langle \hat{a}^\dagger \hat{a} \rangle = -2\epsilon_m \mathrm{Im}\langle \hat{a} \rangle + \kappa\left\langle \hat{a}^\dagger \hat{a} \right\rangle \tag{28h}$$

where we've defined the decoherence rate $\gamma_2 \equiv \frac{1}{2}\gamma_1 + \gamma_\phi$

### 5.3 Purcell Decay

In constructing the Master Equation 27, we've assumed that the dissipator terms are unaffected by the dispersive transformation. This may not necessarily be true. Instead, Ref. [3] derive an alternate master equation within the strong dispersive regime, introducing corrections to the dissipator terms. Particularly, this leads to the Purcell Effect, where the qubit can decay through a photon channel. The Purcell decay rate is given by

$$\gamma_\kappa \approx \frac{g^2}{\Delta^2} n\kappa \tag{29}$$

Intuitively, this can be understood as the qubit excitation partly living in the cavity. From Equation 5, the dressed state $|n_+\rangle$ corresponds to a nearly excited qubit. However, with the system in such a state there is a probability of $ng^2/\Delta^2$ that the excitation is instead found in the cavity. Multiplying this probability with the photon-decay rate approximately gives the Purcell decay rate.

## 6 Measurement in Circuit QED

Circuit QED has several advantages to offer over previous technique, such as single-electron detection in close proximity to the qubit [2]. As stated by Ref [2] these advantages are:

1. Excellent Measurement ON/OFF Ratio: Measurement only occurs in the presence of a probe tone. In the absence of the probe tone, backaction of the cavity on the qubit is avoided by the fact that they're off-resonant.

2. Necessary Dissipation Occurs Away from the Qubit: Measurement necessarily involves non-unitary dissipation. With circuit QED this dissipation happens at some voltmeter at room temp, rather than at a device fabricated around the qubit. Moreover, the dispersive regime ensures that the probe-tone photons aren't absorbed by the qubit. This results in a Quantum Non-Demolition

measurement (i.e. when the qubit stays in the $|0\rangle$ or $|1\rangle$ state, respectively, during and after the measurement; only backaction induced by the measurement is the necessary dephasing of the superposition state).

### 6.1 Microwave Field Detection

Figure 6.1 shows a schematic for the microwave field detection. The following discussion is adapted from Ref. [2]

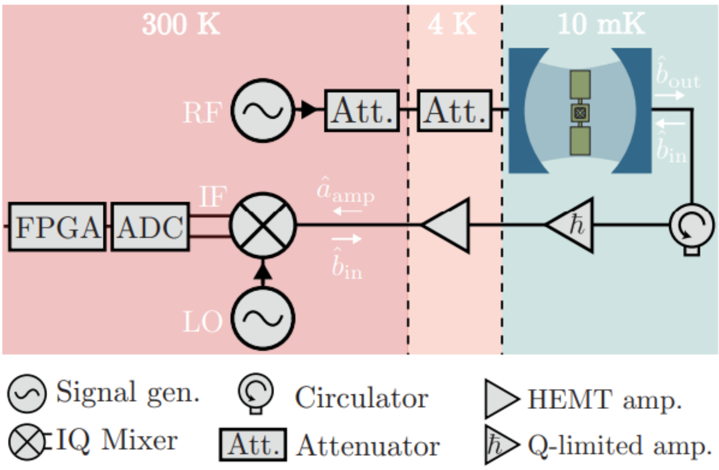


Figure 4: Schematic representation of the microwave measurement chain for field detection in circuit QED, with the resonator depicted as a Fabry-Perot cavity (Sourced from Ref. [2]).

Step 1: An RF signal is applied to the input port of the resonator, after being attenuated to reduce the thermal radiation. We can define this signal as a classical AC voltage with amplitude $A_{RF}$, frequency $\omega_{RF}$, and phase $\phi_{LO}$:

$$V_{RF}(t) = A_{RF}\cos(\omega_{RF}t - \phi_{LO})$$

Step 2: The circulator isolates the field into ($\hat{b}_{in}(t)$) and out of ($\hat{b}_{out}(t)$) the resonator's output port. $\hat{b}_{out}$ is sent to a series of amplifiers, whereas $\hat{b}_{out}$ is suppressed by a dummy output.

In practice the various components have a finite bandwidth. Let's assume that it is wider than bandwidth of the signal of interest, $\hat{b}_{out}(t)$. To account for this finite bandwidth, we can consider the filtered output signal $\hat{a}_f(t)$.

$$\begin{aligned}
\hat{a}_f(t) &= (f * \hat{b}_{out})(t) \\
&= \int_{-\infty}^{\infty} f(t-\tau)\,\hat{b}_{out}(\tau)\,d\tau \\
&= \int_{-\infty}^{\infty} f(t-\tau)\,\left[\sqrt{\kappa}\hat{a}(\tau) + \hat{b}_{in}(\tau)\right]\,d\tau
\end{aligned}$$

where we've used the boundary condition: $\hat{b}_{out} - \hat{b}_{in} = \sqrt{\kappa}\hat{b}$. This means that the field outside the cavity is equal to the intra-cavity field that has left the cavity; since photon decay happens at a rate $\kappa$, then the field ought to decay at $\sqrt{\kappa}$.

The filter function is normalized to $\int_{-\infty}^{\infty}|f(t)|dt = 1$, such that $\left[\hat{b}_f(t), \hat{b}_f^\dagger(t)\right] = 1$.

Step 3: The output field is amplified by a quantum limited amplifier first and then by a HEMT (High Electron Mobility Transfer) amplifier.

Assuming the amplifiers are phase preserving (i.e. they amplify both quadratures equally), we have that the field leaving the amplifiers, $\hat{a}_{amp}$ is:

$$\hat{a}_{amp} = \sqrt{G}\,\hat{a}_f + \sqrt{G-1}\,\hat{h}^\dagger$$

where $G$ is the power gain and $\hat{h}^\dagger$ represents the noise added by the amplifier (known as idler noise). Note that the bosonic commutation relation is preserved.

$$\left[\hat{a}_{amp}, \hat{a}_{amp}^\dagger\right] = G\left[\hat{a}_f, \hat{a}_f^\dagger\right] + (G-1)\left[\hat{h}^\dagger, \hat{h}\right] = G - (G-1) = 1$$

Since the I and Q quadratures are canonically conjugate, amplification without noise would violate the Heisenberg Uncertainty Principle. This point is discussed in detail in Section 6.2

The voltage after amplification is

$$\begin{aligned}
\hat{V}_{amp}(t) &= \sqrt{\frac{\hbar\omega_{RF} Z_{tml}}{2}}\left(\hat{a}_{amp} e^{-i\omega_{RF} t} + \hat{a}_{amp}^\dagger e^{+i\omega_{RF} t}\right) \\
&= \sqrt{\frac{G\hbar\omega_{RF} Z_{tml}}{2}}\left(\hat{a}_f e^{-i\omega_{RF} t} + \hat{a}_f^\dagger e^{+i\omega_{RF} t}\right) + \hat{V}_{amp,noise} \\
&= \sqrt{\frac{G\hbar\omega_{RF} Z_{tml}}{2}}\left[(\hat{a}_f^\dagger + \hat{a}_f)\cos(\omega_{RF} t) + i(\hat{a}_f^\dagger - \hat{a}_f)\sin(\omega_{RF} t)\right] + \hat{V}_{amp,noise}
\end{aligned}$$

define the conjugate operators $\hat{X}_f \equiv \mathrm{Re}\{\hat{a}_f\} = \dfrac{\hat{a}_f^\dagger + \hat{a}_f}{2}$, and $\hat{P}_f \equiv \mathrm{Im}\{\hat{a}_f\} = i\dfrac{\hat{a}_f^\dagger - \hat{a}_f}{2}$

$$\hat{V}_{amp}(t) = \sqrt{2G\hbar\omega_{RF} Z_{tml}}\left[\hat{X}_f\cos(\omega_{RF} t) + \hat{P}_f\sin(\omega_{RF} t)\right] + \hat{V}_{amp,noise} \tag{30}$$

Step 4: The signal is mixed with the local oscillator (LO), digitized by an ADC and processed with an FPGA.

The goal of the IQ-Mixer is to isolate the $\hat{X}_f$ and $\hat{P}_f$ data from the $\hat{V}_{amp}$ signal. The $\hat{X}_f$ and $\hat{P}_f$ data amplitude modulates signals that are a $\frac{\pi}{2}$ out-of-phase apart. In other words, $\hat{V}_{amp}$ is a linear combination of two linearly independent signals. To do this lets consider multiplying an arbitrary signal $A_{RF}\cos(\omega_{RF} t - \phi_{RF})$, with a local oscillator $A_{LO}\cos(\omega_{LO} t - \phi_{LO})$.

$$\begin{aligned}
&A_{RF}\cos(\omega_{RF} t - \phi_{RF}) \cdot A_{LO}\cos(\omega_{LO} t - \phi_{LO}) \\
&\quad = \frac{1}{2}A_{RF}A_{LO}\left[\cos\Big((\omega_{RF} - \omega_{LO})t - (\phi_{RF} - \phi_{LO})\Big) + \cos\Big((\omega_{RF} + \omega_{LO})t - (\phi_{RF} + \phi_{LO})\Big)\right] \\
&\quad \xrightarrow{\text{Lo-Pass Filter}} \frac{1}{2}A_{RF}A_{LO}\cos\Big((\omega_{RF} - \omega_{LO})t - (\phi_{RF} - \phi_{LO})\Big)
\end{aligned}$$

The lo-pass filtered signal oscillates at an intermediate frequency (IF) $\omega_{IF} = \omega_{RF} - \omega_{LO}$, with a phase $\phi_{IF} = \phi_{RF} - \phi_{LO}$.

From Equation 30, observe that $\phi_{RF} = 0$ or $\frac{\pi}{2}$ for the $\hat{X}_f$ and $\hat{P}_f$ respectively. As such, we can set the coefficients on the $\hat{X}_f$ or $\hat{P}_f$ signals to 0 or 1 by multiplying with an in-phase or quadrature local oscillator.

$$\begin{aligned}
\hat{V}_{mixer,I} &= V_{IF}\left[\hat{X}_f\cos(\omega_{RF} t)\cos(\omega_{LO} t) + \hat{P}_f\sin(\omega_{RF} t)\cos(\omega_{LO} t)\right] + \hat{V}_{noise,I} \\
&\xrightarrow{\text{Lo-Pass Filter}} V_{IF}\left[\hat{X}_f\cos(\omega_{IF} t) + \hat{P}_f\sin(\omega_{IF} t)\right] + \hat{V}_{noise,I}
\end{aligned} \tag{31}$$

$$\begin{aligned}
\hat{V}_{mixer,Q} &= V_{IF}\left[\hat{X}_f\cos(\omega_{RF} t)\sin(\omega_{LO} t) + \hat{P}_f\sin(\omega_{RF} t)\sin(\omega_{LO} t)\right] + \hat{V}_{noise,Q} \\
&\xrightarrow{\text{Lo-Pass Filter}} V_{IF}\left[-\hat{X}_f\sin(\omega_{IF} t) + \hat{P}_f\cos(\omega_{IF} t)\right] + \hat{V}_{noise,Q}
\end{aligned} \tag{32}$$

where all noise is accumulated in $\hat{V}_{noise,I/Q}$, the amplitude is represented as $V_{IF} = KA_{LO}\sqrt{GZ_{tml}\hbar\omega_{RF}/2}$, and $K$ represents the conversion losses.

A Homodyne Measurement sets $\boxed{\omega_{RF} = \omega_{LO}}$. In other words, $\omega_{IF} = 0$, simply making the $\hat{V}_{mixer,I} = V_{IF}\hat{X}_f + \hat{V}_{noise,I}$ and $\hat{V}_{mixer,Q} = V_{IF}\hat{P}_f + \hat{V}_{noise,Q}$. However, the measured signal is purely in DC, making it succeptible to 1/f noise and drift.

To correct this, a Heterodyne Measurement leaves the signal to oscillate at $\omega_{IF}$. In other words, the $\hat{V}_{amp,I/Q}$ rotate in the $\hat{X}_f$-$\hat{P}_f$ plane at the frequency $\omega_{IF}$, as shown in Figure 6.1. To extract the $\hat{X}_f$-$\hat{P}_f$, we can rotate the vectors by $-\omega_{IF}t$ (in other words, switch to a frame rotating at $\omega_{IF}$).

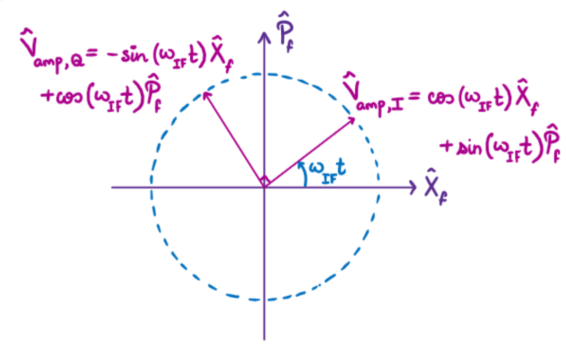


Figure 5: The I-Q signals measured with a heterodyne measurement rotate in the $\hat{X}_f$-$\hat{P}_f$ plane at the frequency $\omega_{IF}$.

## 6.2 Notes on Noise and the Heisenberg Uncertainty Principle

Being able to measure a non-Hermitian operator $\hat{a}_f$ is equivalent to measuring the non-commuting operators $\hat{X}_f = \mathrm{Re}\{\hat{a}_f\}$ and $\hat{P}_f = \mathrm{Im}\{\hat{a}_f\}$. This is seemingly a violation of the Heisenberg Uncertainty Principle.

The added noise terms $\hat{V}_{noise,I/Q}$ are crucial for avoiding this paradox. They allow us to measure both the position and momentum values, with an associated uncertainty. This can be further understood by representing the IQ mixer as a beam-splitter, shown in Figure 6.2. The inputs to the beam-splitter, $\hat{a}_{amp}$ and $\hat{v}$, should be completely unrelated. As such $\hat{a}_{amp}$ and $\hat{v}$ must commute. Since the beam splitting is a unitary, the I and Q quadratures leaving the mixer must be commuting operators as well. This allows us to simultaneously measure them both.

## 6.3 Dispersive Readout of the Steady State Field

This derivation follows the discussion from Ref. [2], Section V.C.1.

For a pulsed measurement, we initialize the qubit in $|g\rangle$ or $|e\rangle$ and then have a constant measurement pulse. i.e. $\Omega_d(t) = 0$ and $\epsilon_m(t) = \epsilon$.

Observe that the cavity frequency is dependant on the state of the qubit. As pointed out by Ref. [2], this setup resembles the Stern-Gerlach experiment. There, the magnetic field gradient entagles the spin state of the atom with the linear momentum of the atom. Thus, measuring the final position of the atom on the detector uniquely identifies the spin state of the atom, provided there isn't any overlap between the final position distributions for the two spin states. This effectively performs a projective measurement of the spin. Similarly, a measurement of the cavity field resolves the state of the qubit. Moreover, since $\hat{H}_{disp}$ commutes with $\hat{\sigma}_z$ this is a Quantum Non-Demolition experiment (as opposed to the Stern-Gerlach experiment, which is destructive). This means any

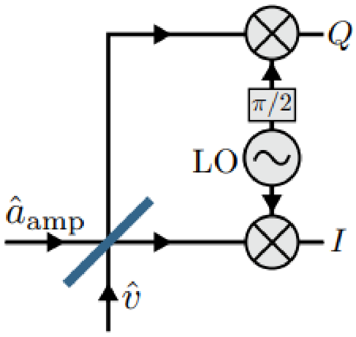


Figure 6: Schematic representation of an IQ mixer as a beam-splitter. This representation accounts for the splitting of the signal $\hat{a}_{amp}$, as well as the added vacuum noise (due to internal modes). The two outputs are combined with a local oscillator (LO) at mixers. By phase shifting the LO by $\pi/2$ in one of the two arms, it is possible to simultaneously measure the two quadratures of the field. Sourced from Ref. [2].

back-action induced by the measurement is in collapsing a qubit superposition in superposition of $|g\rangle$ and $|e\rangle$, into one of the measurement eigenstates. The "QND-ness" of the measurement ensures that subsequent measurements aren't random, but reproduce the first measurement result.

The first CBE (Equation 28a) gives the time-evolution of the cavity field. We can state that the qubit is in an eigenstate, such that $\hat{\sigma}_z = \pm 1$, and consider the system in steady state, $\frac{d}{dt}\hat{a}(t) = 0$.

$$\boxed{\langle \hat{a} \rangle_{g/e} = \frac{-i\epsilon}{\frac{\kappa}{2} - i(\Delta_{cm} \mp \chi)} = \left[\frac{-\epsilon}{(\Delta_{cm} \mp \chi)^2 + \left(\frac{\kappa}{2}\right)^2}\right]\left[\Delta_{cm} \mp \chi + i\frac{\kappa}{2}\right]} \tag{33}$$

Thus the expected cavity field would just be one of two points in the IQ, depending on the qubit state. The uncertainty in $\langle \hat{a} \rangle$ causes the response to appear as "blobs" around the expectation value. The Wigner functions of these responses show coherent states centered around $\langle \hat{a} \rangle_{g/e}$ [2].

To increase the fidelity of single-shot readout, we must reduce the overlap between the two coherent states. The separation between the two coherent states should depend linearly on the measurement amplitude.

$$\langle \hat{a} \rangle_g - \langle \hat{a} \rangle_e = \frac{2\epsilon\chi}{\chi^2 - (\Delta_{cm} - i\frac{\kappa}{2})^2} \tag{34}$$

The square of the expected amplitude is,

$$\boxed{|\langle \hat{a} \rangle_{g/e}|^2 = \frac{\epsilon^2}{(\Delta_{cm} \mp \chi)^2 + (\frac{\kappa}{2})^2}} \tag{35}$$

In frequency space, this quantity is a Lorentzian with an amplitude of $\epsilon^2\pi/\kappa$ and a linewidth of $\kappa$. The Lorentzian is centered at $\omega_m = \omega_r \mp \chi$ for the qubit in $|g\rangle$ or $|e\rangle$ respectively. This reflects the interpretation in Section 3.1, that the cavity frequency is pulled to $\omega_r \mp \chi$ depending on qubit state.

Similarly, the expected phase shift is,

$$\boxed{\phi_{g/e} \equiv \arctan\left(\frac{\mathrm{Re}\{\langle \hat{a} \rangle_{g/e}\}}{\mathrm{Im}\{\langle \hat{a} \rangle_{g/e}\}}\right) = \arctan\left(\frac{\Delta_r \mp \chi}{\kappa/2}\right)} \tag{36}$$

Therefore, the phase shift is a step which drops at $\omega_m = \omega_r \mp \chi$ with respect to the qubit state. For a small linewidth $\kappa$, we expect a very sharp step.

Figure 7 shows the transmission (dashed lines) and phase-shift (solid lines) spectra for the qubit in the ground (blue) and excited (red) states [2].

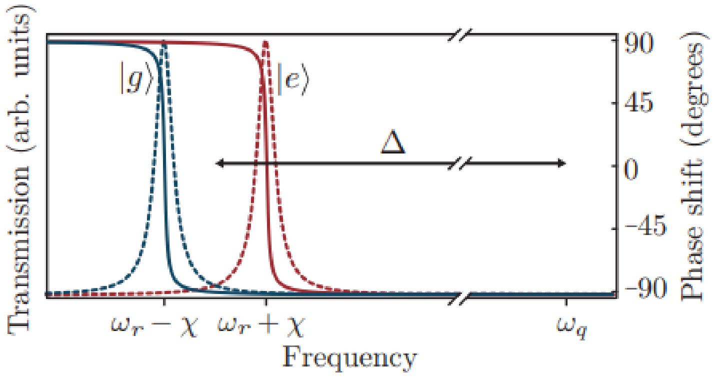


Figure 7: Resonator transmission (dashed lines) and corresponding phase shifts (full lines) for the two qubit states (blue: ground; red: excited). When driving the resonator close to its pulled frequencies, the resonator response strongly depends on the state of the qubit. Sourced from Ref. [2]

### 6.4 Cavity Population as a Function of Drive Power

The mean photon number in the cavity is proportional to the square of the expected amplitude of the coherent state, $|\langle \hat{a} \rangle_{g/e}|^2$, as given by Equation 35. However, as we saw earlier, the complete diagonalization alludes that the cavity frequency shifts as it gets populated. Therefore, the results from the previous section would only be valid at $\bar{n} \ll n_{crit}$ [2, 7].

Ref. [7] derives the change in the cavity frequency and mean photon numbers as function of the drive power, by iteratively calculating both quantities. Figure 6.4 shows their results, for a model with the qubit as a two-level system (in panels (a) and (d)), three-level system (in (c) and (e)), and a six-level system (in (c) and (f)). They show that the cavity frequency and photon number depends on the qubit state (subscript $i$) as well.

Let's consider the two-level system model. Here, we can see that at higher powers, the cavity pull suddenly reduces to zero, and the cavity responds as though ignoring the qubit. This is coupled with the mean cavity population steeply increasing by several orders of magnitude at a power of 40 dB.

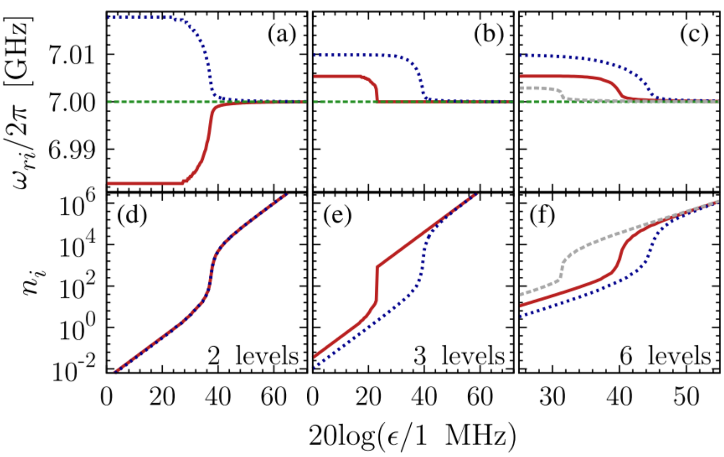


Figure 8: The cavity resonant frequency, $\omega_{ri}$ and the mean photon number, $n_i$ as a function of the drive power, derived by Ref. [7]. The figure shows results from a model with the qubit as a two-level system (in panels (a) and (d)), three-level system (in (c) and (e)), and a six-level system (in (c) and (f)). The solid red, dotted blue, and dashed gray lines [only in (c) and (f)] shows trends when the qubit is in the $|g\rangle$, $|e\rangle$, or $|f\rangle$ states, respectively. In panels (a) through (c), The dashed green line shows the bare cavity frequency. Sourced from [7].

# 7 Qubit Spectroscopy

## 7.1 Qubit Spectrum for a Vacuum Cavity

If we state that $\langle \hat{a}^\dagger \hat{a} \rangle = 0$ and consider the system in steady state $\dot{\rho} = 0$, then the Cavity-Bloch equations corresponding to the qubit state become

$$0 = \frac{\mathrm{d}}{\mathrm{d}t}\langle \hat{\sigma}_z \rangle = \Omega_d \langle \hat{\sigma}_y \rangle - \gamma_1 (1 + \langle \hat{\sigma}_z \rangle) \tag{37a}$$

$$0 = \frac{\mathrm{d}}{\mathrm{d}t}\langle \hat{\sigma}_x \rangle = -\left(\Delta_{qd} + \chi\right) \langle \hat{\sigma}_y \rangle - \gamma_2 \langle \hat{\sigma}_x \rangle \tag{37b}$$

$$0 = \frac{\mathrm{d}}{\mathrm{d}t}\langle \hat{\sigma}_y \rangle = \left(\Delta_{qd} + \chi\right) \langle \hat{\sigma}_x \rangle - \Omega_d \langle \hat{\sigma}_z \rangle - \gamma_2 \langle \hat{\sigma}_y \rangle \tag{37c}$$

Solving these equations simultaneously, we can derive the steady-state population of the qubit $P_e$ [2]. This derivation is described in detail in Appendix E.

$$\boxed{P_e = 1 - P_g = \frac{\langle \hat{\sigma}_z \rangle + 1}{2} = \frac{\Omega_d^2/2}{(\gamma_1/\gamma_2)(\Delta_{qd} + \chi)^2 + \gamma_1\gamma_2 + \Omega_d^2}} \tag{38}$$

The steady state qubit population, $P_e$ has a Lorentzian lineshape with respect to the drive frequency on the qubit $\omega_d$. The Lorentzian is centered at the Lamb-shifted qubit frequency $\omega_q + \chi$.

In the limit of a strong qubit drive i.e. a large $\Omega_d$, the steady-state qubit population saturates at $P_e = P_g = \frac{1}{2}$ [2].

The qubit spectrum has a linewidth (full width at half maximum), $\gamma_q$, given by Equation 39.

$$\boxed{\gamma_q = 2\sqrt{\frac{\gamma_2}{\gamma_1}\Omega_d^2 + \gamma_2^2}} \tag{39}$$

The linewidth of the qubit spectrum is therefore dependant on the following:

1. Power Broadening: As the qubit drive power is increased from zero, the linewidth of the spectrum expands from $2\gamma_2$ to the quantity given by 39. This can intuitively be understood by considering the driven Hamiltonian of an undamped qubit:

$$\hat{H}_q = \frac{\Delta_{qd}}{2}\hat{\sigma}_z + \frac{\Omega_d}{2}\hat{\sigma}_x$$

When the qubit is driven far away from its resonant frequency, i.e. $\Delta_{qd} >> \Omega_d$, then the qubit vector mostly rotates around Z-axis of the Bloch Sphere. As such, the qubit's population is nearly unchanged. However, as we increase the drive power $\Omega_d^2$, we can rotate the qubit-vector around the X-axis even when the qubit-drive is sufficiently detuned from the resonant frequency.

2. Qubit Relaxation, $T_1 = 1/\gamma_1$: $T_1$ causes the qubit to rotate around the X-axis of the Bloch sphere as well. The factor $\frac{\gamma_2}{\gamma_1} = \frac{1}{2} + \frac{\gamma_\phi}{\gamma_1}$ demonstrates the competing rates of rotation around the X and Z axes, induced by environmental damping.

3. Qubit Decoherence, $T_2 = 1/\gamma_2$: As mentioned earlier, the unbroadened spectrum has a linewidth of $2\gamma_2 = 2T_2$. In practice, the qubit's $T_2$ is determined from a Ramsey-fringe or Hahn-Echo experiment [2].

4. Finite Width Pulses: Just as with pulses on the cavity, we can't have an infinitely long constant tone on the qubit. Instead, we excite the qubit with a long square pulse, that approximates

a constant drive. Following a similar explanation as with the cavity, we see a wider sinc-like function when the pulse length, $\tau_d$ is short compared to the the qubit's timescale $1/\gamma_q$. As we increase $\tau_d$, the oscillations induced by the sinc dissapear and we can begin to recover the Lorentzian.

Intuitively, shorter square pulses are comprised of a wider range of frequencies. Thus pulses which are detuned from the resonant frequency still have a non-zero component of the resonant frequency. As such, these pulses are still able to excite the qubit to some extent.

## 7.2 AC-Stark Shift and Measurement-Induced Dephasing

In the previous discussion, we assumed that the cavity is in its vacuum state, i.e. $\langle \hat{a}^\dagger \hat{a} \rangle \to 0$. However, carrying out the above derivation with for a constant cavity population $\langle \hat{a}^\dagger \hat{a} \rangle = \bar{n}$, leads to the qubit frequency being shifted by an average value of $2\chi\bar{n}$.

The shift in the qubit frequency depending on $\bar{n}$ and prior knowledge of $\chi$, allows one to infer the intra-cavity population as a function of the measurement power [8, 2]. However, as stated to in Section 3.2, the linear cavity pull is only valid in the regime where $\bar{n} \ll n_{crit}$. This is discussed in detail in Section 8.

While we've discussed the average shift in the qubit frequency, the actual shift is given by $2\chi\hat{a}^\dagger\hat{a}$, as alluded to by Equation 10. Unlike $\langle \hat{a}^\dagger \hat{a} \rangle$ which may be constant, the measurement of $\hat{a}^\dagger\hat{a}$ is stochastic. Therefore, when the cavity is forced into a coherent state by the measurement tone, each Fock State $|n\rangle$ of the coherent field contributes to its own qubit frequency shift $2\chi n$.

Ref. [5] derive the qubit spectrum under two models.

1. Model 1: Gaussian Approximation for the Photon Shot Noise

Firstly they consider the photon-number statistics as Gaussian noise around the mean photon number $\bar{n}$. This is equivalent to assuming Gaussian noise for the relative phase of the coherent state, as $\Delta N \Delta\phi = \hbar/2$. This assumption results in the qubit absorption spectrum Equation 40 [5].

$$\tilde{S}(\omega) = \frac{1}{2\pi} \sum_{j=0}^{\infty} \frac{(-2\tilde{\gamma}_m/\kappa)^j}{j!} \frac{\tilde{\gamma}_j/2}{(\Delta_{qd} + 2\chi\left[\bar{n} + \frac{1}{2}\right])^2 + (\tilde{\gamma}_j/2)^2} \tag{40}$$

where $\tilde{\gamma}_m = 2\kappa\bar{n}\left[\arctan(2\chi/\kappa)\right]^2 \approx 8\chi^2\bar{n}/\kappa$ is the measurement-induced dephasing rate, $\tilde{\gamma}_j = 2(\gamma_2 + \tilde{\gamma}_m) + j\kappa$ is the linewidth for the $j^{th}$ Lorentzian.

Therefore, in this model, the qubit spectrum is given as a sum of Lorentzians, all of which are centered around the *mean AC-Stark shift frequency.* The the Lorentzians are scaled by a Poissonian-like distribution (up to a factor) with mean $2\tilde{\gamma}_m/\kappa$. The linewidth of the Lorentzians increases linearly with the index $j$.

If the measurement induced dephasing rate $\tilde{\gamma}_m$ is much smaller than the cavity decay rate $\kappa/2$, then the mean of the Poisson distribution is small and the qubit spectrum essentially comprises of terms with smaller linewidths. Therefore, the spectrum is has a Lorentzian lineshape, where the linewidth scales with $\bar{n}$ [2].

On the other hand, if $\tilde{\gamma}_m \gg \kappa/2$, then the qubit spectrum consists of more terms [2], each with a wider linewidth, resulting in a wider Gaussian-like profile, whose linewidth scales as $\sqrt{\bar{n}}$. The square root dependance reflects the coherent nature of the cavity field. On the other hand, for a thermally populated cavity a $\bar{n}(\bar{n}+1)$ dependance is observed. The condition $\tilde{\gamma}_m \gg \kappa/2$ can be understood as the qubit dephasing before the cavity has time to reach steady state [5, 2].

Since, $\tilde{\gamma}_m$ is proportional to $\bar{n}$, we expect a Lorentzian-like lineshape for $\bar{n} \ll (\kappa/4\chi)^2$ and a Gaussian-like lineshape for $\bar{n} \gg (\kappa/4\chi)^2$. The broadening of the qubit spectrum due to the mean

[2]The variance of a Poissonian distribution is directly proportional to its mean.

cavity population is known as *Measurement Induced Dephasing* [5, 2].

The AC Stark shift and measurement induced dephasing effects are both shown in 7.2(a). Observe that as the cavity population increases, qubit peak broadens and is shifted by $2\chi\langle\hat{a}^\dagger\hat{a}\rangle$.

2. Model 2: Positive P-Integration of the Master Eqaution

Model 1 only considers the *average* qubit frequency shift, $2\chi\langle\hat{a}^\dagger\hat{a}\rangle$. However, the actual shift is given by $2\chi\hat{a}^\dagger\hat{a}$ [2]. As such the true photon number statistics are relevant. As such, Ref [5] are motivated to go beyond the Gaussian approximation by integrating the Master Equation given by 27.

Using a *Polaron Transformation*, the cavity is eliminated out of the Master Equation, and the measurement induced dephasing rate in the dispersive regime is expressed as

$$\gamma_m(t) = -2\chi\mathrm{Im}[\langle\hat{a}\rangle_g(t)\langle\hat{a}\rangle_e^*(t)]$$

In the long time limit, the measurement induced dephasing rate is proportional to the distance between the two coherent states [5]. Intuitively, if the measurement becomes more projective in the qubit's $\hat{\sigma}_z$ basis, then "more information flows out of the qubit" and it dephases faster.

$$\begin{aligned}\gamma_m &= \frac{\kappa}{2}|\langle\hat{a}\rangle_e - \langle\hat{a}\rangle_g|^2 \\ &= \frac{\kappa\chi^2(\bar{n}_g + \bar{n}_e)}{\Delta_{cm}^2 + \chi^2 + (\kappa/2)^2}\end{aligned} \tag{41}$$

where $\bar{n}_{g/e} = |\langle\hat{a}^\dagger\hat{a}\rangle|$ is the average cavity population depending on the qubit state. If we take $\Delta_{rm} = 0$, then $\bar{n}_g = \bar{n}_e \equiv \bar{n}$ for a TLS and $\gamma_m$ scales linearly with $\bar{n}$.

In this model, the qubit spectrum is given by Equation 42 [5].

$$S(\omega) = \frac{1}{\pi}\sum_{j=0}^{\infty}\mathrm{Re}\left\{\frac{\mu^j e^{-\mu}}{j!}\frac{1}{\gamma_j/2 - i(\omega-\omega_j)}\right\} \tag{42}$$

$$\begin{aligned}\text{where } \gamma_j &= 2(\gamma_2 + \gamma_m) + j\kappa \\ \omega_j &= (\omega_q + \chi) + \chi(\bar{n}_g + \bar{n}_e) - \frac{2\chi}{\kappa}\gamma_m + j(\chi + \Delta_{cm}) \\ \mu &= 2\gamma_m\left(\frac{1}{\kappa} - \frac{1}{\kappa/2 + i(\Delta_{cm} + \chi)}\right)\end{aligned}$$

In general, the spectrum is a sum of Lorentzians with linewidths $\gamma_j$. However, unlike the result from Method 1, Equation 42 describes an asymmetric qubit spectrum as each Lorentzian is peaked at its own frequency $\omega_j$. The spectral amplitudes are distributed with a Poissonian distribution with mean $\mu$.

When $\chi \gg \kappa$, then the seperation between the peaks is much greater than the individual linewidths. As shown in Figure 7.2(b), the qubit peaks corresponding to AC Stark Shifts by each Fock State $|n\rangle$, are spectroscopically discernable. Moreover, as $\mu \to 2\gamma_m/\kappa$ the mean AC Stark shifted frequency is given by the more familiar result from Method 1.

$$\begin{aligned}\bar{\omega} &= (\omega_q + \chi) + \chi(2\bar{n}) - \frac{2\chi}{\kappa}\gamma_m + \mu\chi \qquad (\text{at } \Delta_{cm} = 0\ ) \\ &= (\omega_q + \chi) + 2\chi\bar{n} - \frac{2\chi}{\kappa}\gamma_m + \chi\left(\frac{2\gamma_m}{\kappa}\right) \\ &= \omega_q + 2\chi\left(\bar{n} + \frac{1}{2}\right)\end{aligned}$$

On the other hand, when $\chi \lessapprox \kappa$, the results from this method resemble those from Method 1.

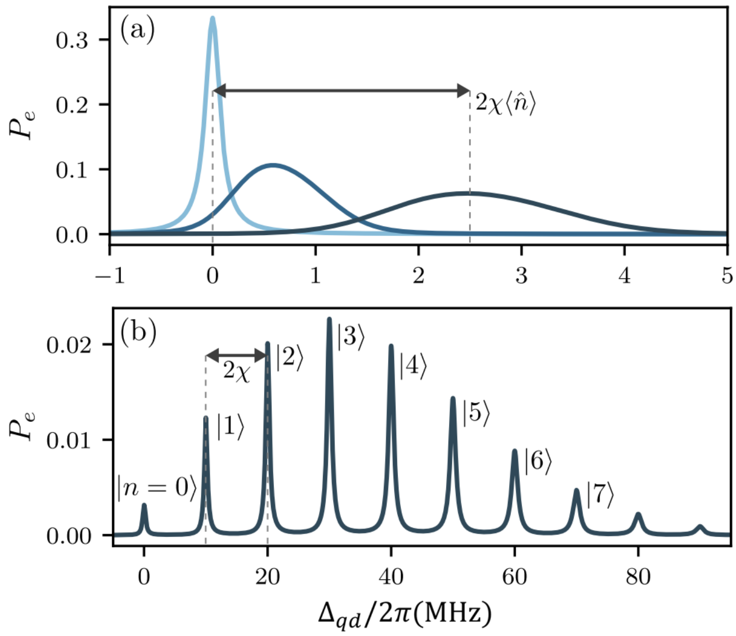


Figure 9: Excited state population as a function of the qubit drive frequency. For a system in the (a) weak dispersive regime with $\chi/2\pi = 0.1$ MHz and (b) strong dispersive regime with $\chi/2\pi = 5$ MHz. (a) Shows the qubit peak broadening due to measurement induced dephasing, whereas (b) shows the number-splitting of the qubit spectrum. The resolved peaks in (b) correspond to different cavity photon numbers. In both plots, the spectroscopy drive amplitude is fixed to $\Omega_d/2\pi = 0.1$ MHz and the damping rates are $\gamma_1/2\pi = \kappa/2\pi = 0.1$ MHz. In (a) the measurement drive is on resonance with the bare-cavity frequency (i.e. $\Delta_{cm} = 0$) with an amplitude of $\epsilon_m \in \{0, 0.2, 0.4\}$ MHz for the light blue, blue, and dark blue lines, respectively. In (b) the measurement drive is at the pulled cavity frequency (i.e. $\Delta_{cm} = \chi$ with an amplitude of $\epsilon/2\pi = 0.1$ MHz) (Sourced from Ref. [2]).

This is because (at $\Delta_{cm} = 0$),

$$\gamma_m = 2\bar{n}\kappa \left( \frac{1}{\left(\frac{\kappa/2}{\chi}\right)^2 + 1} \right) \longrightarrow \frac{8\bar{n}\chi^2}{\kappa} = \tilde{\gamma}_m$$

$$\mu \longrightarrow \frac{2\gamma}{\kappa} \approx \frac{2\tilde{\gamma}_m}{\kappa} \qquad\qquad \omega_j \longrightarrow \omega_q + 2\chi\left(\bar{n} + \frac{1}{2}\right)$$

Figure 7.2 shows the qubit spectrum as a function of $\chi/\kappa$. As this parameter is increased, the Gaussian approximation breaks down and we enter the "*Number Splitting Regime*", where the individual spectral peaks are discernable.

# 8 Experiments with HouckLab - Calibrating the Mean Photon Number

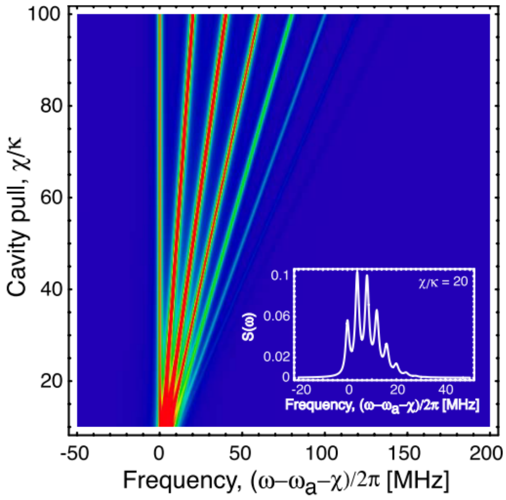


Figure 10: The spectrum $S(\omega)$, given by Equation 42, as a function of $\chi/\kappa$. The measurement tone is detuned at $\Delta_{cm} = \chi$, such that the cavity is always driven at the ground-state pulled frequency, $\omega_c - \chi$. The dephasing rate is set to $\gamma_2 = 7.6\kappa$ and the average photon number is set to $\bar{n} = 2$. Inset: Spectrum at $\chi/\kappa = 20$, where number-splitting should be observable. Sourced from Ref. [5].

# Appendix A Commutator Relations

$$[\hat{a}, \hat{a}^\dagger] = 1 \qquad [\hat{a}, \hat{a}^\dagger\hat{a}] = \hat{a} \qquad [\hat{a}^\dagger, \hat{a}^\dagger\hat{a}] = -\hat{a}^\dagger$$
$$[\hat{\sigma}_+, \hat{\sigma}_-] = \hat{\sigma}_z \qquad [\hat{\sigma}_\pm, \hat{\sigma}_z] = \mp 2\hat{\sigma}_\pm \qquad [\hat{\sigma}_i, \hat{\sigma}_j] = 2\epsilon_{ijk}\hat{\sigma}_k$$

where $i, j \in \{x, y, z\}$ and $\epsilon_{ijk}$ is the Levi-Cavita tensor.

# Appendix B Derivation of the Dispersive Hamiltonian in the Linear Regime

As stated in Section 3.1, we choose $\hat{S} = \frac{g}{\Delta}\hat{V}_- = \frac{g}{\Delta}\left(\hat{\sigma}_+\hat{a} - \hat{\sigma}_-\hat{a}^\dagger\right)$, such that $[\hat{H}_0, \hat{S}] = \hbar g\hat{V}_+$.

$$\begin{aligned}
[\hat{H}_0, \hat{S}] &= \frac{1}{2}\hbar\omega_q\left[\hat{\sigma}_z, \frac{g}{\Delta}\left(\hat{\sigma}_+\hat{a} - \hat{\sigma}_-\hat{a}^\dagger\right)\right] + \hbar\omega_c\left[\hat{a}^\dagger\hat{a} - \frac{1}{2}, \frac{g}{\Delta}\left(\hat{\sigma}_+\hat{a} + \hat{\sigma}_-\hat{a}^\dagger\right)\right] \\
&= \frac{1}{2}\hbar\omega_q \cdot \frac{g}{\Delta}\left([\hat{\sigma}_z, \hat{\sigma}_+]\hat{a} - [\hat{\sigma}_z, \hat{\sigma}_-]\hat{a}^\dagger\right) + \hbar\omega_c \cdot \frac{g}{\Delta}\left(\hat{\sigma}_+[\hat{a}^\dagger\hat{a}, \hat{a}] - \hat{\sigma}_-[\hat{a}^\dagger\hat{a}, \hat{a}^\dagger]\right) \\
&= \hbar\omega_q \cdot \frac{g}{\Delta}\left(\hat{\sigma}_+\hat{a} + \hat{\sigma}_-\hat{a}^\dagger\right) + \hbar\omega_c \cdot \frac{g}{\Delta}\left(-\hat{\sigma}_+\hat{a} - \hat{\sigma}_-\hat{a}^\dagger\right) \\
&= \hbar\left(\omega_q - \omega_c\right) \cdot \frac{g}{\Delta}\left(\hat{\sigma}_+\hat{a} + \hat{\sigma}_-\hat{a}^\dagger\right) \\
&= \hbar g\hat{V}_+
\end{aligned}$$

Then, using the Baker-Campbell-Haussdorf formula, we can expand $\hat{H}'$ in terms of the small parameter $\frac{g^2}{\Delta}$.

$$
\begin{aligned}
\hat{H}' &= \hat{H} + [\hat{S}, \hat{H}] + \frac{1}{2!}[\hat{S}, [\hat{S}, \hat{H}]] + \frac{1}{3!}[\hat{S}, [\hat{S}, [\hat{S}, \hat{H}]]] + \dots \\
&= \left(\hat{H}_0 + \hbar g \hat{V}_+\right) + \hbar \left(-g\hat{V}_+ + \frac{g^2}{\Delta}[\hat{V}_-, \hat{V}_+]\right) + \frac{1}{2}\hbar \left(-\frac{g^2}{\Delta}[\hat{V}_-, \hat{V}_+] + \left(\frac{g^2}{\Delta}\right)^2 [\hat{V}_-, [\hat{V}_-, \hat{V}_+]]\right) \\
&\qquad + \mathcal{O}\left(\left(\frac{g^2}{\Delta}\right)^2\right) \\
&= \hat{H}_0 + \frac{\hbar g^2}{2\Delta}[\hat{V}_-, \hat{V}_+] + \mathcal{O}\left(\left(\frac{g^2}{\Delta}\right)^2\right) \\
&\approx \hat{H}_0 + \frac{\hbar g^2}{2\Delta}\Big[\left(\hat{\sigma}_+\hat{a} - \hat{\sigma}_-\hat{a}^\dagger\right), \left(\hat{\sigma}_+\hat{a} + \hat{\sigma}_-\hat{a}^\dagger\right)\Big] \\
&= \hat{H}_0 + \frac{1}{2}\hbar\chi\left([\hat{\sigma}_+\hat{a}, \hat{\sigma}_-\hat{a}^\dagger] - [\hat{\sigma}_-\hat{a}^\dagger, \hat{\sigma}_+\hat{a}]\right) \qquad \text{where } \chi \equiv \frac{g^2}{\Delta} \\
&= \hat{H}_0 + \hbar\chi[\hat{\sigma}_+\hat{a}, \hat{\sigma}_-\hat{a}^\dagger] \\
&= \hat{H}_0 - \hbar\chi\left(\hat{\sigma}_z\hat{a}^\dagger\hat{a} + \hat{\sigma}_+\hat{\sigma}_-\right) \\
&= \hat{H}_0 - \hbar\chi\left(\hat{\sigma}_z\hat{a}^\dagger\hat{a} + \frac{1}{2}\left(\hat{\sigma}_z + \hat{\mathbb{1}}\right)\right)
\end{aligned}
$$

This gives the dispersive Hamiltonian to first order in $\chi = \frac{g^2}{\Delta}$ (as in Equation 9).

$$
\boxed{\hat{H}_{disp} = \frac{1}{2}\hbar\omega_q\hat{\sigma}_z - \hbar\left(\omega_c + \chi\hat{\sigma}_z\right)\left(\hat{a}^\dagger\hat{a} + \frac{1}{2}\right) - \frac{1}{2}\hbar\chi} \tag{43}
$$

# Appendix C Derivation of the Exact Diagonalization of the Dispersive Hamiltonian

As stated in 3.2, the following derivation is inspired by Ref. [3].

Just as in the Linear Regime, the anti-Hermitian operator $V_-$ is key for this diagonalization. The total excitation number $\hat{N} = \hat{a}^\dagger\hat{a} + \hat{\sigma}_+\hat{\sigma}_-$ is also important, as it commutes with $\hat{H}$ as well as $\hat{V}_-$. We set $\hat{S} = f(\hat{N})\hat{V}_-$, where $f$ is the function to be determined.

Recall from the Linear Regime that $[\hat{V}_-, \hat{H}_0] = -\hbar\Delta\hat{V}_+$. Using this result, the unitary transformation of $\hat{H}$ by $e^{\hat{S}}$ yields

$$
\begin{aligned}
\hat{H}' = &\left(\hat{H}_0 + \hbar g\hat{V}_+\right) + f(\hat{N})\left([\hat{V}_-, \hat{H}] + \hbar g[\hat{V}_-, \hat{V}_+]\right) + \frac{1}{2!}f^2(\hat{N})\left([\hat{V}_-, [\hat{V}_-, \hat{H}_0]] + \hbar g[\hat{V}_-, [\hat{V}_-, \hat{V}_+]]\right) \\
&\qquad + \frac{1}{3!}f^3(\hat{N})\left([\hat{V}_-, [\hat{V}_-, [\hat{V}_-, \hat{H}_0]] + \hbar g[\hat{V}_-, [\hat{V}_-, [\hat{V}_-, \hat{V}_+]]]]\right) + \dots \\
= &\ \hat{H}_0 + \hbar\left(g - f(\hat{N})\Delta\right)\hat{V}_+ + \hbar f(\hat{N})\left(\frac{2g - f(\hat{N})\Delta}{2!}\right)[\hat{V}_-, \hat{V}_+] \\
&\qquad + \hbar f^2(\hat{N})\left(\frac{3g - f(\hat{N})\Delta}{3!}\right)[\hat{V}_-, [\hat{V}_-, \hat{V}_+]] + \dots
\end{aligned}
$$

We can use the results from the Linear Regime to simplify the commutator terms involving $\hat{V}_-$ and $\hat{V}_+$.

$$[\hat{V}_-, \hat{V}_+] = -2\left(\hat{\sigma}_z \hat{a}^\dagger \hat{a} + \hat{\sigma}_+ \hat{\sigma}_-\right) = -2\left(\hat{a}^\dagger \hat{a} + \hat{\sigma}_+ \hat{\sigma}_-\right)\hat{\sigma}_z = -2\hat{N}\hat{\sigma}_z$$

$$[\hat{V}_-, [\hat{V}_-, \hat{V}_+]] = -2\hat{N}[\hat{V}_-, \hat{\sigma}_z] = -2\hat{N}\left([\hat{\sigma}_+, \hat{\sigma}_z]\hat{a} - [\hat{\sigma}_-, \hat{\sigma}_z]\hat{a}^\dagger\right) = 4\hat{N}\hat{V}_+$$

$$[\hat{V}_-, [\hat{V}_-, [\hat{V}_-, \hat{V}_+]]] = 4\hat{N}[\hat{V}_-, \hat{V}_+] = -2(4)\hat{N}^2\hat{\sigma}_z$$

$$[\hat{V}_-, [\hat{V}_-, [\hat{V}_-, [\hat{V}_-, \hat{V}_+]]]] = -2(4)\hat{N}^2[\hat{V}_-, \hat{\sigma}_z] = 4^2\hat{N}^2\hat{V}_+$$

In general,

$$\underbrace{[\hat{V}_-, [\hat{V}_-, [\hat{V}_-, \ldots, \hat{V}_+]]]}_{2m \text{ times}} = 4^m \hat{N}^m \hat{V}_+ = \left(2\sqrt{\hat{N}}\right)^{2m} \hat{V}_+$$

$$\underbrace{[\hat{V}_-, [\hat{V}_-, [\hat{V}_-, [\hat{V}_-, \ldots, \hat{V}_+]]]]}_{2m+1 \text{ times}} = -2(4)^m \hat{N}^{m+1}\hat{\sigma}_z = -2\hat{N}\left(2\sqrt{\hat{N}}\right)^{2m} \hat{\sigma}_z$$

Using this result, we can write $\hat{H}'$ as

$$\begin{aligned}
\hat{H}' &= \hat{H}_0 + \hbar\left[\sum_{m=0}^{\infty}\left(\frac{(2m+1)g - f\Delta}{(2m+1)!}\right)\left(2f\sqrt{\hat{N}}\right)^{2m}\right]\hat{V}_+ \\
&\quad - 2\hbar\hat{N}\left[\sum_{m=0}^{\infty}\left(\frac{2(m+1)g - f\Delta}{2(m+1)!}\right)\left(2f\sqrt{\hat{N}}\right)^{2m+1}\right]\hat{\sigma}_z \\
&= \hat{H}_0 + \hbar\left[\frac{\Delta\sin(2f\sqrt{\hat{N}})}{2\sqrt{\hat{N}}} + g\cos(2f\sqrt{\hat{N}})\right]\hat{V}_+ \\
&\quad - 2\hbar\hat{N}\left[\frac{g\sin(2f\sqrt{\hat{N}})}{2\sqrt{\hat{N}}} + \frac{\Delta[1-\cos(2f\sqrt{\hat{N}})]}{4\hat{N}}\right]\hat{\sigma}_z
\end{aligned}$$

To complete the diagonalization we choose

$$f(\hat{N}) = \frac{-\arctan(2\frac{g}{\Delta}\sqrt{\hat{N}})}{2\sqrt{\hat{N}}}$$

such that the off-diagonal interaction term proportional to $\hat{V}_+$ is eliminated. Finally, we get the exact diagonal form as:

$$\boxed{\hat{H}' = \hat{H}_0 - \frac{1}{2}\hbar\Delta\left(1 - \sqrt{1 + 4\hat{N}\left(\frac{g}{\Delta}\right)^2}\right)\hat{\sigma}_z} \tag{44}$$

# Appendix D Derivation of the Cavity Bloch Equations

Before we dive into the physics, consider the following lemmas.

**Lemma D.1.** *For any pair of operators $\hat{A}$ and $\hat{B}$ acting on a system described by the density matrix $\hat{\rho}$,*

$$\textit{trace}([\hat{B}, \hat{\rho}]\hat{A}) = \langle[\hat{A}, \hat{B}]\rangle$$

*Proof:*

$$\begin{aligned}
\mathrm{trace}([\hat{B},\hat{\rho}]\hat{A}) &= \mathrm{trace}(\hat{B}\hat{\rho}\hat{A} - \hat{\rho}\hat{B}\hat{A}) \\
&= \mathrm{trace}(\hat{B}\hat{\rho}\hat{A}) - \mathrm{trace}(\hat{\rho}\hat{B}\hat{A}) \\
&= \mathrm{trace}(\hat{\rho}\hat{A}\hat{B}) - \mathrm{trace}(\hat{\rho}\hat{B}\hat{A}) \qquad \text{using the circular property of trace} \\
&= \mathrm{trace}(\hat{\rho}(\hat{A}\hat{B} - \hat{B}\hat{A})) \\
&= \langle[\hat{A},\hat{B}]\rangle
\end{aligned}$$

□

**Lemma D.2.** *For any pair of operators $\hat{A}$ and $\hat{B}$ acting on a system described by the density matrix $\hat{\rho}$,*

$$\mathit{trace}(\mathcal{D}[\hat{B}]\hat{\rho}\ \hat{a}) = \left\langle \hat{B}^\dagger\hat{a}\hat{B} - \frac{1}{2}\hat{A}\hat{B}^\dagger\hat{B} - \frac{1}{2}\hat{B}^\dagger\hat{B}\hat{A}\right\rangle$$

*Proof:*

$$\begin{aligned}
\mathrm{trace}(\mathcal{D}[\hat{B}]\hat{\rho}\ \hat{A}) &= \mathrm{trace}\left(\hat{B}\hat{\rho}\hat{B}^\dagger\hat{A} - \frac{1}{2}\hat{B}^\dagger\hat{B}\hat{\rho}\hat{A} - \frac{1}{2}\hat{\rho}\hat{B}^\dagger\hat{B}\hat{a}\right) \\
&= \mathrm{trace}(\ \hat{B}\hat{\rho}\hat{B}^\dagger\hat{A}\ ) - \frac{1}{2}\mathrm{trace}(\ \hat{B}^\dagger\hat{B}\hat{\rho}\hat{A}\ ) - \frac{1}{2}\mathrm{trace}(\ \hat{\rho}\hat{B}^\dagger\hat{B}\hat{A}\ ) \\
&= \mathrm{trace}(\ \hat{\rho}\hat{B}^\dagger\hat{A}\hat{B}\ ) - \frac{1}{2}\mathrm{trace}(\ \hat{\rho}\hat{A}\hat{B}^\dagger\hat{B}\ ) - \frac{1}{2}\mathrm{trace}(\ \hat{\rho}\hat{B}^\dagger\hat{B}\hat{A}\ ) \\
&= \mathrm{trace}\left(\hat{\rho}\left(\hat{B}^\dagger\hat{A}\hat{B} - \frac{1}{2}\hat{A}\hat{B}^\dagger\hat{B} - \frac{1}{2}\hat{B}^\dagger\hat{B}\hat{a}\right)\right) \\
&= \left\langle \hat{B}^\dagger\hat{A}\hat{B} - \frac{1}{2}\hat{A}\hat{B}^\dagger\hat{B} - \frac{1}{2}\hat{B}^\dagger\hat{B}\hat{A}\right\rangle
\end{aligned}$$

□

Now, let's consider the time-evolution of expectation value of an operator $\hat{a}$. Let's only consider time-invariant operators i.e. $\frac{\mathrm{d}}{\mathrm{d}t}\hat{a} = 0$. Then,

$$\frac{\mathrm{d}}{\mathrm{d}t}\langle\hat{a}\rangle = \frac{\mathrm{d}}{\mathrm{d}t}\mathrm{trace}(\hat{\rho}\hat{a}) = \mathrm{trace}(\dot{\hat{\rho}}\hat{a})$$

The Master equation gives the expression for $\dot{\hat{\rho}}$. Expanding the trace for each term and using Lemmas D.1 and D.2, obtain equation 45.

$$\begin{aligned}
\frac{\mathrm{d}}{\mathrm{d}t}\langle\hat{a}\rangle = &-\frac{i}{\hbar}\langle[\hat{a},\hat{H}]\rangle + \kappa\left\langle \hat{a}^\dagger\hat{a}\hat{a} - \frac{1}{2}\hat{a}\hat{a}^\dagger\hat{a} - \frac{1}{2}\hat{a}^\dagger\hat{a}\hat{a}\right\rangle \\
&+ \gamma_1\left\langle \hat{\sigma}_+\hat{a}\hat{\sigma}_- - \frac{1}{2}\hat{a}\hat{\sigma}_+\hat{\sigma}_- - \frac{1}{2}\hat{\sigma}_+\hat{\sigma}_-\hat{a}\right\rangle + \gamma_\phi\left\langle \hat{\sigma}_z\hat{a}\hat{\sigma}_z - \frac{1}{2}\hat{a}\hat{\sigma}_z^2 - \frac{1}{2}\hat{\sigma}_z^2\hat{a}\right\rangle
\end{aligned} \tag{45}$$

Particularly, observe that if $\hat{a}$ is just in the photonic Hilbert space, then the $3^{rd}$ and $4^{th}$ terms vanish. Similarly, if $\hat{a}$ is just in the qubit's Hilbert space, then the $2^{nd}$ term vanishes.

If we go into a rotating frame with $U(t) = \exp(\hbar\omega_m\hat{a}^\dagger\hat{a} + \frac{1}{2}\omega_s\hat{\sigma}_z)$, then we can just use the Hamiltonian in this frame, given by Equation 46.

$$\frac{\hat{H}'}{\hbar} = \left(\frac{\Delta_{as}+\chi}{2}\right)\hat{\sigma}_z + (\Delta_{cm} + \chi\hat{\sigma}_z)\hat{a}^\dagger\hat{a} + \epsilon_m(t)(\hat{a}+\hat{a}^\dagger) +_d (t)\hat{\sigma}_x \tag{46}$$

In this frame, the CBEs follow directly from Equation 45. The first CBE describes the evolution of the photonic-annihilation operator. Using Equation 45, we have that

$$\begin{aligned}
\frac{\mathrm{d}}{\mathrm{d}t}\langle\hat{a}\rangle &= -\frac{i}{\hbar}\langle[\hat{a},\hat{H}]\rangle + \frac{\kappa}{2}\left\langle\hat{a}^\dagger\hat{a}^2 - \hat{a}\hat{a}^\dagger\hat{a}\right\rangle \\
&= -i\Delta_{cm}\langle[\hat{a},\hat{a}^\dagger\hat{a}]\rangle - i\chi\langle[\hat{a},\hat{\sigma}_z\hat{a}^\dagger\hat{a}]\rangle - i\epsilon_m + \frac{\kappa}{2}\left\langle[\hat{a}^\dagger,\hat{a}]\hat{a}\right\rangle \\
&= -i\Delta_{cm}\langle\hat{a}\rangle - i\chi\langle\hat{a}\hat{\sigma}_z\rangle - i\epsilon_m + \frac{\kappa}{2}\langle\hat{a}\rangle
\end{aligned}$$

Similarly, we can derive second CBE from the paper, which describes the evolution of the Pauli-Z matrix.

$$\begin{aligned}
\frac{\mathrm{d}}{\mathrm{d}t}\langle\hat{\sigma}_z\rangle &= -\frac{i}{\hbar}\langle[\hat{\sigma}_z,\hat{H}]\rangle + \gamma_1\left\langle\hat{\sigma}_+\hat{\sigma}_z\hat{\sigma}_- - \frac{1}{2}\hat{\sigma}_z\hat{\sigma}_+\hat{\sigma}_- - \frac{1}{2}\hat{\sigma}_+\hat{\sigma}_-\hat{\sigma}_z\right\rangle \\
&= -i\chi\langle[\hat{\sigma}_z,\hat{\sigma}_z\hat{a}^\dagger\hat{a}]\rangle - i\Omega_d\langle[\hat{\sigma}_z,\hat{\sigma}_x]\rangle + \gamma_1\left\langle(2|e\rangle\langle e|)\right\rangle \\
&= \Omega_d\langle\hat{\sigma}_y\rangle - \gamma_1\langle\hat{\mathbb{1}}+\hat{\sigma}_z\rangle \\
&= \Omega_d\langle\hat{\sigma}_y\rangle - \gamma_1(1+\langle\hat{\sigma}_z\rangle)
\end{aligned}$$

Likewise, the evolution of the Pauli-X and Pauli-Y matrices can also be derived from Equation 45. For this derivation, we make the approximation $\langle\hat{a}^\dagger\hat{a}\hat{\sigma}_i\rangle \approx \langle\hat{a}^\dagger\hat{a}\rangle\langle\hat{\sigma}_i\rangle$, as suggested by Ref [6]. This approximation should be valid for low photon numbers, where dephasing caused by photon shot noise is ignored.

$$\begin{aligned}
\frac{\mathrm{d}}{\mathrm{d}t}\langle\hat{\sigma}_x\rangle &= -\frac{i}{\hbar}\langle[\hat{\sigma}_x,\hat{H}]\rangle + \gamma_1\left\langle\hat{\sigma}_+\hat{\sigma}_x\hat{\sigma}_- - \frac{1}{2}\hat{\sigma}_x\hat{\sigma}_+\hat{\sigma}_- - \frac{1}{2}\hat{\sigma}_+\hat{\sigma}_-\hat{\sigma}_x\right\rangle \\
&\qquad + \gamma_\phi\left\langle\hat{\sigma}_z\hat{\sigma}_x\hat{\sigma}_z - \frac{1}{2}\hat{\sigma}_x\hat{\sigma}_z^2 - \frac{1}{2}\hat{\sigma}_z^2\hat{\sigma}_x\right\rangle \\
&= -i\chi\langle[\hat{\sigma}_x,\hat{\sigma}_z\hat{a}^\dagger\hat{a}]\rangle - i\left(\frac{\Delta_{as}+\chi}{2}\right)\langle[\hat{\sigma}_x,\hat{\sigma}_z]\rangle - \frac{\gamma_1}{2}\langle\hat{\sigma}_x\rangle - \gamma_\phi\langle\hat{\sigma}_x\rangle \\
&= -i\chi\langle[\hat{\sigma}_x,\hat{\sigma}_z]\hat{a}^\dagger\hat{a}\rangle - (\Delta_{as}+\chi)\langle\hat{\sigma}_y\rangle - \left(\frac{\gamma_1}{2}+\gamma_\phi\right)\langle\hat{\sigma}_x\rangle \\
&= -2\chi\langle\hat{a}^\dagger\hat{a}\hat{\sigma}_y\rangle - (\Delta_{as}+\chi)\langle\hat{\sigma}_y\rangle - \left(\frac{\gamma_1}{2}+\gamma_\phi\right)\langle\hat{\sigma}_x\rangle \\
&\approx -\left[\Delta_{as}+2\chi\left(\langle\hat{a}^\dagger\hat{a}\rangle+\frac{1}{2}\right)\right]\langle\hat{\sigma}_y\rangle - \left(\frac{\gamma_1}{2}+\gamma_\phi\right)\langle\hat{\sigma}_x\rangle
\end{aligned}$$

$$\begin{aligned}
\frac{\mathrm{d}}{\mathrm{d}t}\langle\hat{\sigma}_y\rangle &= -\frac{i}{\hbar}\langle[\hat{\sigma}_x,\hat{H}]\rangle + \gamma_1\left\langle\hat{\sigma}_+\hat{\sigma}_y\hat{\sigma}_- - \frac{1}{2}\hat{\sigma}_y\hat{\sigma}_+\hat{\sigma}_- - \frac{1}{2}\hat{\sigma}_+\hat{\sigma}_-\hat{\sigma}_y\right\rangle \\
&\qquad + \gamma_\phi\left\langle\hat{\sigma}_z\hat{\sigma}_y\hat{\sigma}_z - \frac{1}{2}\hat{\sigma}_y\hat{\sigma}_z^2 - \frac{1}{2}\hat{\sigma}_z^2\hat{\sigma}_y\right\rangle \\
&= -i\chi\langle[\hat{\sigma}_y,\hat{\sigma}_z\hat{a}^\dagger\hat{a}]\rangle - i\left(\frac{\Delta_{as}+\chi}{2}\right)\langle[\hat{\sigma}_y,\hat{\sigma}_z]\rangle - i\Omega_d\langle[\hat{\sigma}_y,\hat{\sigma}_x]\rangle - \frac{\gamma_1}{2}\langle\hat{\sigma}_x\rangle - \gamma_\phi\langle\hat{\sigma}_x\rangle \\
&= -i\chi\langle[\hat{\sigma}_y,\hat{\sigma}_z]\hat{a}^\dagger\hat{a}\rangle + (\Delta_{as}+\chi)\langle\hat{\sigma}_x\rangle - \Omega_d\langle\hat{\sigma}_z\rangle - \left(\frac{\gamma_1}{2}+\gamma_\phi\right)\langle\hat{\sigma}_y\rangle \\
&= 2\chi\langle\hat{a}^\dagger\hat{a}\hat{\sigma}_x\rangle + (\Delta_{as}+\chi)\langle\hat{\sigma}_y\rangle - -\Omega_d\langle\hat{\sigma}_z\rangle - \left(\frac{\gamma_1}{2}+\gamma_\phi\right)\langle\hat{\sigma}_y\rangle \\
&\approx \left[\Delta_{as}+2\chi\left(\langle\hat{a}^\dagger\hat{a}\rangle+\frac{1}{2}\right)\right]\langle\hat{\sigma}_x\rangle - \Omega_d\langle\hat{\sigma}_z\rangle - \left(\frac{\gamma_1}{2}+\gamma_\phi\right)\langle\hat{\sigma}_y\rangle
\end{aligned}$$

We can now look at the product terms $\langle\hat{a}\hat{\sigma}_i\rangle$, as described by equations 5(e), 5(f) and 5(g) from the paper. For this derivation, we make the approximation $\langle\hat{a}^\dagger\hat{a}\hat{a}\hat{\sigma}_i\rangle \approx \langle\hat{a}^\dagger\hat{a}\rangle\langle\hat{a}\hat{\sigma}_i\rangle$, as suggested by Ref [6].

$$
\begin{aligned}
\frac{\mathrm{d}}{\mathrm{d}t}\langle\hat{a}\hat{\sigma}_z\rangle &= -\frac{i}{\hbar}\langle[\hat{a}\hat{\sigma}_z, H]\rangle + \frac{\kappa}{2}\left\langle \hat{a}^\dagger\hat{a}^2\hat{\sigma}_z - \hat{a}\hat{a}^\dagger\hat{a}\hat{\sigma}_z\right\rangle \\
&\quad + \gamma_1\left\langle \hat{a}\hat{\sigma}_+\hat{\sigma}_z\hat{\sigma}_- - \frac{1}{2}\hat{a}\hat{\sigma}_z\hat{\sigma}_+\hat{\sigma}_- - \frac{1}{2}\hat{a}\hat{\sigma}_+\hat{\sigma}_-\hat{\sigma}_z\right\rangle \\
&= -i\Delta_{cm}\langle[\hat{a}\hat{\sigma}_z, \hat{a}^\dagger\hat{a}]\rangle - i\chi\langle[\hat{a}\hat{\sigma}_z, \hat{\sigma}_z\hat{a}^\dagger\hat{a}]\rangle - i\epsilon_m\langle[\hat{a}\hat{\sigma}_z, \hat{a}^\dagger]\rangle \\
&\quad - i\Omega_d\langle[\hat{a}\hat{\sigma}_z, \hat{\sigma}_x]\rangle + \frac{\kappa}{2}\left\langle[\hat{a}^\dagger, \hat{a}]\hat{a}\hat{\sigma}_z\right\rangle + \gamma_1\left\langle \hat{a} + \hat{a}\hat{\sigma}_z\right\rangle \\
&= -i\Delta_{cm}\langle\hat{a}\hat{\sigma}_z\rangle - i\chi\langle\hat{a}\rangle + \Omega_d\langle\hat{a}\hat{\sigma}_y\rangle - i\epsilon_m\langle\hat{\sigma}_z\rangle - \gamma_1\langle\hat{a}\rangle - \left(\gamma_1 + \frac{\kappa}{2}\right)\langle\hat{a}\hat{\sigma}_z\rangle
\end{aligned}
$$

$$
\begin{aligned}
\frac{\mathrm{d}}{\mathrm{d}t}\langle\hat{a}\hat{\sigma}_x\rangle &= -\frac{i}{\hbar}\langle[\hat{a}\hat{\sigma}_x, H]\rangle + \frac{\kappa}{2}\left\langle \hat{a}^\dagger\hat{a}^2\hat{\sigma}_x - \hat{a}\hat{a}^\dagger\hat{a}\hat{\sigma}_x\right\rangle \\
&\quad + \gamma_1\left\langle \hat{a}\hat{\sigma}_+\hat{\sigma}_x\hat{\sigma}_- - \frac{1}{2}\hat{a}\hat{\sigma}_x\hat{\sigma}_+\hat{\sigma}_- - \frac{1}{2}\hat{a}\hat{\sigma}_+\hat{\sigma}_-\hat{\sigma}_x\right\rangle + \gamma_\phi\left\langle \hat{a}\hat{\sigma}_z\hat{\sigma}_x\hat{\sigma}_z - \frac{1}{2}\hat{a}\hat{\sigma}_x\hat{\sigma}_z^2 - \frac{1}{2}\hat{a}\hat{\sigma}_z^2\hat{\sigma}_x\right\rangle \\
&= -i\Delta_{cm}\langle[\hat{a}\hat{\sigma}_x, \hat{a}^\dagger\hat{a}]\rangle - i\chi\langle[\hat{a}\hat{\sigma}_x, \hat{\sigma}_z\hat{a}^\dagger\hat{a}]\rangle - i\left(\frac{\Delta_{as}+\chi}{2}\right)\langle[\hat{a}\hat{\sigma}_x, \hat{\sigma}_z]\rangle \\
&\quad - i\epsilon_m\langle[\hat{a}\hat{\sigma}_x, \hat{a}^\dagger]\rangle + \frac{\kappa}{2}\left\langle[\hat{a}^\dagger, \hat{a}]\hat{a}\hat{\sigma}_x\right\rangle - \frac{\gamma_1}{2}\langle\hat{a}\hat{\sigma}_x\rangle - \gamma_\phi\langle\hat{a}\hat{\sigma}_x\rangle \\
&= -i\Delta_{cm}\langle\hat{a}\hat{\sigma}_x\rangle - \chi\langle\hat{a}\hat{a}^\dagger\hat{a}\hat{\sigma}_y\rangle - \chi\langle\hat{a}^\dagger\hat{a}\hat{a}\hat{\sigma}_y\rangle - (\Delta_{as}+\chi)\langle\hat{a}\hat{\sigma}_y\rangle \\
&\quad - i\epsilon_m\langle\hat{\sigma}_x\rangle - \left(\frac{\kappa}{2} + \frac{\gamma_1}{2} + \gamma_\phi\right)\langle\hat{a}\hat{\sigma}_x\rangle \\
&\approx -i\Delta_{cm}\langle\hat{a}\hat{\sigma}_x\rangle - [\Delta_{as} + 2\chi(\langle\hat{a}^\dagger\hat{a}\rangle + 1)]\langle\hat{a}\hat{\sigma}_y\rangle - i\epsilon_m\langle\hat{\sigma}_x\rangle - \left(\frac{\kappa}{2} + \frac{\gamma_1}{2} + \gamma_\phi\right)\langle\hat{a}\hat{\sigma}_x\rangle
\end{aligned}
$$

$$
\begin{aligned}
\frac{\mathrm{d}}{\mathrm{d}t}\langle\hat{a}\hat{\sigma}_y\rangle &= -\frac{i}{\hbar}\langle[\hat{a}\hat{\sigma}_y, H]\rangle + \frac{\kappa}{2}\left\langle \hat{a}^\dagger\hat{a}^2\hat{\sigma}_y - \hat{a}\hat{a}^\dagger\hat{a}\hat{\sigma}_y\right\rangle \\
&\quad + \gamma_1\left\langle \hat{a}\hat{\sigma}_+\hat{\sigma}_y\hat{\sigma}_- - \frac{1}{2}\hat{a}\hat{\sigma}_y\hat{\sigma}_+\hat{\sigma}_- - \frac{1}{2}\hat{a}\hat{\sigma}_+\hat{\sigma}_-\hat{\sigma}_y\right\rangle + \gamma_\phi\left\langle \hat{a}\hat{\sigma}_z\hat{\sigma}_y\hat{\sigma}_z - \frac{1}{2}\hat{a}\hat{\sigma}_y\hat{\sigma}_z^2 - \frac{1}{2}\hat{a}\hat{\sigma}_z^2\hat{\sigma}_y\right\rangle \\
&= -i\Delta_{cm}\langle[\hat{a}\hat{\sigma}_y, \hat{a}^\dagger\hat{a}]\rangle - i\chi\langle[\hat{a}\hat{\sigma}_y, \hat{\sigma}_z\hat{a}^\dagger\hat{a}]\rangle - i\left(\frac{\Delta_{as}+\chi}{2}\right)\langle[\hat{a}\hat{\sigma}_y, \hat{\sigma}_z]\rangle \\
&\quad - i\epsilon_m\langle[\hat{a}\hat{\sigma}_y, \hat{a}^\dagger]\rangle - i\Omega_d\langle[\hat{\sigma}_y, \hat{\sigma}_x]\rangle + \frac{\kappa}{2}\left\langle[\hat{a}^\dagger, \hat{a}]\hat{a}\hat{\sigma}_y\right\rangle - \frac{\gamma_1}{2}\langle\hat{a}\hat{\sigma}_y\rangle - \gamma_\phi\langle\hat{a}\hat{\sigma}_y\rangle \\
&= -i\Delta_{cm}\langle\hat{a}\hat{\sigma}_y\rangle + \chi\langle\hat{a}\hat{a}^\dagger\hat{a}\hat{\sigma}_x\rangle + \chi\langle\hat{a}^\dagger\hat{a}\hat{a}\hat{\sigma}_x\rangle - (\Delta_{as}+\chi)\langle\hat{a}\hat{\sigma}_x\rangle \\
&\quad - i\epsilon_m\langle\hat{\sigma}_y\rangle - \Omega_d\langle\hat{a}\hat{\sigma}_z\rangle - \left(\frac{\kappa}{2} + \frac{\gamma_1}{2} + \gamma_\phi\right)\langle\hat{a}\hat{\sigma}_x\rangle \\
&\approx -i\Delta_{cm}\langle\hat{a}\hat{\sigma}_x\rangle + [\Delta_{as} + 2\chi(\langle\hat{a}^\dagger\hat{a}\rangle + 1)]\langle\hat{a}\hat{\sigma}_y\rangle - i\epsilon_m\langle\hat{\sigma}_x\rangle - \Omega_d\langle\hat{a}\hat{\sigma}_z\rangle \\
&\quad - \left(\frac{\kappa}{2} + \frac{\gamma_1}{2} + \gamma_\phi\right)\langle\hat{a}\hat{\sigma}_x\rangle
\end{aligned}
$$

Finally, let's derive the time-evolution of the expectation value of the photon-number operator $\langle\hat{a}^\dagger\hat{a}\rangle$.

$$
\begin{aligned}
\frac{\mathrm{d}}{\mathrm{d}t}\langle \hat{a}^\dagger\hat{a}\rangle &= -\frac{i}{\hbar}\langle[\hat{a}^\dagger\hat{a},\hat{H}]\rangle + \kappa\left\langle \hat{a}^{\dagger 2}\hat{a}^2 - (\hat{a}^\dagger\hat{a})^2\right\rangle \\
&= -i\chi\langle[\hat{a}^\dagger\hat{a},\hat{\sigma}_z\hat{a}^\dagger\hat{a}]\rangle - i\epsilon_m\langle[\hat{a}^\dagger\hat{a},\hat{a}^\dagger+\hat{a}]\rangle + \kappa\left\langle \hat{a}^\dagger[\hat{a}^\dagger,\hat{a}]\hat{a}\right\rangle \\
&= -i\epsilon_m\langle\hat{a}-\hat{a}^\dagger\rangle + \kappa\left\langle\hat{a}^\dagger\hat{a}\right\rangle \\
&= -2\epsilon_m\mathrm{Im}\langle\hat{a}\rangle + \kappa\left\langle\hat{a}^\dagger\hat{a}\right\rangle
\end{aligned}
$$

This gives the complete set of Cavity-Bloch Equations (equation 28), which exactly match Ref [6].

# Appendix E Derivation of the Qubit Spectrum for a Vacuum Cavity

The simultaneous equations stated by Equation 37 can be rearranged as in Equation 47

$$\Omega_d\langle\hat{\sigma}_y\rangle = \gamma_1(1+\langle\hat{\sigma}_z\rangle) \tag{47a}$$

$$(\Delta_{qd}+\chi)\langle\hat{\sigma}_y\rangle = -\gamma_2\langle\hat{\sigma}_x\rangle \tag{47b}$$

$$(\Delta_{qd}+\chi)\langle\hat{\sigma}_x\rangle = \Omega_d\langle\hat{\sigma}_z\rangle + \gamma_2\langle\hat{\sigma}_y\rangle \tag{47c}$$

Inserting, 47(a) into (b) and (c), we can eliminate $\langle\hat{\sigma}_y\rangle$.

$$\langle\hat{\sigma}_x\rangle = \frac{-\gamma_1}{\gamma_2\Omega_d}(\Delta_{qd}+\chi)(1+\langle\hat{\sigma}_z\rangle) \tag{48a}$$

$$(\Delta_{qd}+\chi)\langle\hat{\sigma}_x\rangle = \Omega_d\langle\hat{\sigma}_z\rangle + \frac{\gamma_1\gamma_2}{\Omega_d}(1+\langle\hat{\sigma}_z\rangle) \tag{48b}$$

We can now eliminate $\langle\hat{\sigma}_x\rangle$ by substituting 48(a) into (b).

$$
\begin{aligned}
\frac{-\gamma_1}{\gamma_2\Omega_d}(\Delta_{qd}+\chi)^2(1+\langle\hat{\sigma}_z\rangle) &= \Omega_d\langle\hat{\sigma}_z\rangle + \frac{\gamma_1\gamma_2}{\Omega_d}(1+\langle\hat{\sigma}_z\rangle) \\
\left[\frac{\gamma_1}{\gamma_2\Omega_d}(\Delta_{qd}+\chi)^2 + \Omega_d + \frac{\gamma_1\gamma_2}{\Omega_d}\right](1+\langle\hat{\sigma}_z\rangle) &= \Omega_d \\
\left[\frac{\gamma_1}{\gamma_2}(\Delta_{qd}+\chi)^2 + \Omega_d^2 + \gamma_1\gamma_2\right](1+\langle\hat{\sigma}_z\rangle) &= \Omega_d^2
\end{aligned}
$$

Thus, the steady state qubit population, given below, matches Ref. [2].

$$P_e = \frac{1+\langle\hat{\sigma}_z\rangle}{2} = \frac{\Omega_d^2/2}{\left[\frac{\gamma_1}{\gamma_2}(\Delta_{qd}+\chi)^2 + \Omega_d^2 + \gamma_1\gamma_2\right]}$$

# References


[1] Serge Haroche and Jean-Michel Raimond. *"Of Spins and Springs." Exploring the Quantum: Atoms, Cavities and Photons.* Oxford University Press, 2019.

[2] Alexandre Blais, A. Grimsmo, Steve Girvin, and Andreas Wallraff. Circuit quantum electrodynamics. 2020.

[3] Maxime Boissonneault, J. M. Gambetta, and Alexandre Blais. Dispersive regime of circuit qed: Photon-dependent qubit dephasing and relaxation rates. *Phys. Rev. A*, 79:013819, Jan 2009.

[4] P. Krantz, M. Kjaergaard, F. Yan, T. P. Orlando, S. Gustavsson, and W. D. Oliver. A quantum engineer's guide to superconducting qubits. *Applied Physics Reviews*, 6(2):021318, 2019.

[5] Qubit-photon interactions in a cavity: Measurement-induced dephasing and number splitting. 2006.

[6] R Bianchetti, S Filipp, M Baur, J M Fink, M Göppl, P J Leek, L Steffen, A Blais, and A Wallraff. Dynamics of dispersive single-qubit readout in circuit quantum electrodynamics. *Physical Review A*, 80(4):043840, 2009.

[7] Maxime Boissonneault, J M Gambetta, and Alexandre Blais. Improved Superconducting Qubit Readout by Qubit-Induced Nonlinearities. *Physical Review Letters*, 105(10):100504, sep 2010.

[8] D I Schuster, A Wallraff, A Blais, L Frunzio, R.-S Huang, J Majer, S M Girvin, and R J Schoelkopf. ac Stark Shift and Dephasing of a Superconducting Qubit Strongly Coupled to a Cavity Field. *Physical Review Letters*, 94(12):123602, mar 2005.